STABILITY OF SWIRLING FLOW IN PASSIVE CYCLONIC SEPARATOR IN MICROGRAVITY

by

ADEL OMAR KHARRAZ

Submitted in partial fulfillment of the requirements

For the degree of Doctor of Philosophy

Dissertation Advisor: Dr. Y. Kamotani

Department of Mechanical and Aerospace Engineering

CASE WESTERN RESERVE UNIVERSITY

January, 2018

CASE WESTERN RESERVE UNIVERSITY

SCHOOL OF GRADUATE STUDIES

We hereby approve the thesis dissertation of

Adel Omar Kharraz

candidate for the degree of **Doctor of Philosophy***.

Committee Chair

Yasuhiro Kamotani

Committee Member

Jaikrishnan Kadambi

Committee Member

Paul Barnhart

Committee Member

Beverly Saylor

Date of Defense

July 24, 2017

*We also certify that written approval has been obtained

for any proprietary material contained therein.

Dedication

This is for my parents, my wife, and my children.

Table of Contents

List of Tables

List of Figures

Nomenclature

English Symbols

A_{inj}	injector nozzle area
A_{out}	area of liquid outlet
As	separator aspect ratio
C	constant in skin friction formula
C_f	skin friction coefficient
C_α	compression coefficient
D	separator diameter
D_N	injector nozzle diameter
D_{in}	inlet diameter
F_s	surface tension force per unit volume
H	Samsonov configuration height
J_{film}	liquid film angular momentum
J_{in}	flux of angular momentum at injector
J_{out}	flux of angular momentum exiting separator body
K	single-phase backpressure coefficient at the liquid outlet
K_g	two-phase backpressure coefficient at the gas outlet
K_l	two-phase backpressure coefficient at the liquid outlet
L	separator length
L_N	injector nozzle length
M_{wall}	moment caused by viscous stresses at the wall

N	number of cells
Q_{in}	volume flow rate of injected fluid
Q_{out}	volume flow rate of liquid at the liquid outlet
R_1	the larger principle radius of curvature
R_2	the smaller principle radius of curvature
Re_f	liquid film Reynolds number
Re_o	injection Reynolds number
R_i	gas core radius
R_o	separator radius
S	swirl number
U	flow field velocity
U_{in}	velocity at injector nozzle
$U_{l,in}$	liquid velocity at injector nozzle
U_r	relative velocity between gas and liquid phases
U_z	axial velocity at the liquid outlet
U_θ	characteristic azimuthal velocity
We_i	interfacial Weber number
We_o	injection Weber number
a	radial position of interface in hydrodynamic stability
f_b	body force per unit volume
g	gravitational acceleration vector
h	liquid film thickness

$j_{l,in}$	superficial liquid velocity
m	azimuthal mode number
n	exponent in skin friction formula
$\vec{n}$	normal vector to the interface surface
p	pressure
r_i	dimensionless gas core radius
t	time
u	dimensionless characteristic azimuthal velocity
u_z	axial velocity
$u_{\theta,i}$	azimuthal velocity at the interface
u_θ	azimuthal velocity
$\bar{u}_\theta$	dimensionless azimuthal velocity
w	slit width

Greek Symbols

α	void fraction
β	gas volumetric quality of the injected two-phase flow
δ	grid size
Γ	ratio of axially projected area to area of injector nozzle
κ	dimensionless backpressure coefficient
κ_g	dimensionless gas outlet backpressure coefficient
κ_l	dimensionless liquid outlet backpressure coefficient

μ	dynamic viscosity
ν	dimensionless outflow
ν_g	dimensionless gas outflow
ν_l	dimensionless liquid outflow
ρ	density
ρ_g	density of gas phase
ρ_l	density of liquid phase
σ	surface tension
τ	dimensionless time
ϕ	Rayleigh discriminant
χ	curvature of the interface
ω	angular velocity

Acknowledgements

First, all praises to Allah, the Almighty, for providing me strength, knowledge, and understanding to complete this work.

I would like to express sincere gratitude to my thesis advisor, Professor Kamotani, for his guidance, constructive criticism, and most importantly, the long time he spent with me to finish this thesis.

I would also like to thank my department for the financial support with special thanks to Angelika Szakacs who did the major role of making that happen.

I also am indebted to Dr. Yoko Kamotani, for the great efforts she did on editing and proofreading my thesis.

My thanks also goes to Professor Kadambi, Professor Barnhart, and Professor Saylor for generously offering their time to appear on my committee.

I finally would like to express my gratitude to Ming-Fang Kang and Yeyuan Li from the Microgravity Laboratory for the great friendship and assistance.

Stability of Swirling Flow in Passive Cyclonic Separator in Microgravity

Abstract

By

ADEL OMAR KHARRAZ

The use of passive cyclonic separators in microgravity environment to perform phase separation requires taking into account the effect of capillary forces. The study utilizes control-volume approximation and VOF-based CFD simulation to investigate their effects on separator performance in microgravity.

The configuration of liquid film and gas core rotating inside the separator involves the presence of a free surface (interface). In this situation the liquid film thickness becomes very critical because the increase of this film causes an increase in the capillary force at the interface, which may eventually cause a collapse of the liquid film. Therefore an investigation is performed by conducting a parametric study with respect to the dimensionless parameters that represent the separator geometry and the swirling flow hydrodynamics to determine the effects of all of these parameters on the liquid film thickness.

The control-volume approximation in this study is developed using the conservation of mass and angular momentum as well as applying a pressure balance for the separator, taking into account the capillary force effect at the interface. The flow field is assumed to

behave as a solid body rotation. The developed equations are solved to obtain the critical (minimum) Weber number at the interface before collapsing.

The CFD approach utilizes 2-D axisymmetric meshing to discretize the governing equations. OpenFOAM, which is an open source software package, is used to generate the meshing and perform the simulation. The approach is used to develop a skin friction coefficient formula at a low volume flow rate injection which is needed in the control-volume approximation. The flow field is studied with decreasing Weber numbers until the liquid film collapses, which determines the critical Weber number. Also, the effect of contact angle on the liquid film stability is qualitatively investigated using this approach.

Two-phase flow injection is also investigated using only the control-volume approximation. The investigation is carried out at several injection volumetric qualities with the assumption that the void fraction and injection volumetric quality are equal (homogeneous injection).

Chapter 1 Introduction

1.1 Phase Separation Significance in Microgravity

Phase separation is essential in many fluid flow systems in microgravity. While droplet and bubble segregation is a spontaneously occurring phenomenon in most terrestrial situations, a much reduced buoyancy in a microgravity environment often results in situations where two disparate phases have no distinct inclination to separate from one another. This can present many problems with respect to spacecraft and space station operations since proper control and sequestration of the individual phases is often essential to the successful functionality of many system-critical components. In environmental control and life support systems, water processing, reclamation, food cleaning, wastewater recovery, oxygen generation, and humidity control systems are all dependent on separators to contend with multiphase flow phenomena. For example, the use of phase separators to maintain phase purity at the entrances of turbomachinery has often been detailed as a crucial concern (McQuillen et al., 2003). The encroachment of droplets into turbine blades and the resulting destructiveness has, in particular, received much attention (McQuillen, 2004).

Several active and passive gas–liquid separation techniques have been proposed and qualitatively evaluated in the past in order to provide this needed phase separation for microgravity applications. McQuillen et al. (2005) gave an overview of various multiphase flow separators that have been employed. Capillary and membrane approaches have been utilized successfully in space; however, their surfaces are seriously prone to clogging

and have components that frequently must be replaced. Cyclonic (vortex) separation is one technology that exhibits high capability and efficiency in normal gravity usage and have shown promise in microgravity applications (McQuillen, Sankovic, & Hall, 2005). As a device, cyclonic separators have many applications such as Gas Liquid Cylindrical Cyclones (GLCC) in the oil industry (Kouba & Shoham, 1996) and gas cyclones in the coal industry to separate solid particles from gaseous flow (Corte & Gil, 2007). These devices are categorized into passive and active separators. Active separators (also known as rotary separators) require power input to move the rotative separator housing where vortex flow develops and creates a centrifugal force that causes phase separation due to the buoyancy difference. This kind of cyclonic separators demonstrates high separation performance, however; the power requirement and the presence of moving parts make its use in space applications impractical. The other kind of vortex separation is a passive approach. It is classified as being static in the sense that it has no moving parts. This static passivity combined with long-duration operability is the device's greatest advantage compared to the other approaches. The advantages of reliability and requiring no power source highlighted the concern of employing passive cyclonic separators in space applications. The concept that passive cyclonic separators use to segregate phases is similar to the active one, yet the mechanism that leads to create swirling flow is different. In this case, the momentum of the coming injected fluid is utilized to accomplish the task. As the flow is tangentially injected into the separator through an inlet nozzle, the flow gains momentum downstream of the nozzle to develop swirling flow inside the separator compartment. The flow field configuration is a gas core that extends axially along the

device and is surrounded by liquid film. It will be seen later, that the liquid film thickness depends significantly on the injection flow rate. With the increase of liquid film thickness, the surface tension effect increases to become critical and eventually unstable liquid film is experienced which may end to collapsing. As this point of unstable liquid film is the subject of this study, more details will be introduced in the upcoming sections and chapters.

1.2 Effect of Microgravity on Passive Cyclonic Separators

Passive cyclonic separators have received extensive research in terrestrial environment since the 19th century covering most of the science and engineering associated. For micorgravity environment applications, however, a much less knowledge base is available to fully understand the flow hydrodynamics and the fluid physics in such environment. This environment features capillary force which significantly influences the flow fields of pressure and velocity. Capillary force presence is attributed to the rise of surface tension effect in flow fields that characterize low gravity. As a consequence, any attempt of employing these devices in space for instance, requires attentively considering this issue. The efforts in this regard started in the sixties and by the mid of 1990, the pace of research received a notable increase (Hoyt, 2007; Hoyt, 2013) as when NASA began a broad project to investigate in serious manner the effectiveness of using these devices in spacecraft systems for long duration missions such as in regenerative life support systems which require phase separation in some stages. One ambitious attempt was introduced by NASA Glenn Research Center (GRC) in 1995 under device name of Cascade Cyclonic Separation

Device (CSD-C) (Hoyt, 2007; Hoyt, Kamotani, Kadambi, McQuillen, & Sankovic, 2008; McQuillen & Neumann, 1995). In this separator, half of the separator housing has a conical shape wall (frustum section) to gain high separation capability. CFD simulation studies for microgravity have been performed to investigate the separation performance over a wide range of volumetric quality and flow rate. Using modified version of the CSD-C, other extensive ground-based experimentation is carried out at Case Western Reserve University, CWRU, assessing quantitatively steady and transient flow conditions to identify the separator behavior at quite high flow rates (Hoyt, 2013; Hoyt, Kang, Kharraz, Kadambi, & Kamotani, 2011; Hoyt, Kang, Kharraz, Kadambi, & Kamotani, 2012; Hoyt, Kang, Lee, Kharraz, Kadambi, & Kamotani, 2013; Kang, Hoyt, Kadambi, & Kamotani, 2014). The research, however, does not include surface tension effects on the flow field due to the dominance of the inertial force over the capillary force in normal-gravity experimental conditions. In the presence of gravity, Froude number (the centrifugal force to the gravity force ratio) must exceed certain value to hold the liquid film and avoid collapsing. This criterion disables passive separators to work at low injection flow rates in a terrestrial environment which restrains the CWRU research team to undergo experiments to study surface tension effect. Even though, an effort is carried out by the team of employing aircraft parabolic flight at NASA GRC to study CWRU separator in a reduced gravity environment, the test matrix missed including low flow rates which is necessary to observe surface tension effect (Hoyt, 2013). At low flow rate injection the centrifugal force which is caused by the swirling flow becomes low and hence the surface tension forces starts to have more effect on the liquid film. The configuration of the gas core

encircled by liquid film involves forming a free surface (interface) where the surface tension affects the flow field. As Equation 3.1 describes (Young-Laplace equation), the interface curvature and the surface tension as well causes capillary force that produces pressure variation across the interface (pressure jump).

The gas core radius is found in function of the injection flow rate (Hoyt, Kang, Lee, Kharraz, Kadambi, & Kamotani, 2013). At a certain value of low flow rate, the gas core radius reaches critical value where pressure drop due to capillary force starts to cause a significant impact on the interface. Since the flow field inside the separator involves other driving forces that may affect the gas core behavior such as the backpressure at the liquid outlet, additional analysis is required considering all effects. As it will be shown in the later chapters, the rise of capillary force at the interface as the injected flow rate keeps decreasing to lower values will end up to unstable liquid film and eventually the film collapses. That concludes the fact that the interface is very fundamental in phase separation using cyclonic separators in microgravity environment.

1.3 Free Surface (Interface) in Microgravity Environment

The interaction between two immiscible fluids commonly develops free surface as long as adequate circumstances are provided. The flow field configuration in cyclonic separators is one example that is mostly associated with a free surface (interface). The swirling flow in this case develops a free surface between the gas and the liquid. As mentioned earlier, the interface in these devices is prone to the influence of many forces.

In microgravity environment at low flow rates, surface tension plays an important role in affecting the interface. However, this effect decreases as the centrifugal force increases due to higher injection flow rates. To evaluate the effect of these two forces in one versus the other, Weber number is a good measure that compares the centrifugal inertia forces to the surface tension forces. As will be discussed later, Weber number at the interface takes the form of $We_i = \rho u_{\theta,i}^2 R_i/\sigma$. The decrease of interfacial Weber number, either through lowering the injection flow rate or raising the surface tension, yields an unstable liquid film that ends to breakdown in extreme cases. Weber number as a measure to predict the interface stability has been utilized by other researchers (Bean, Waghela, Kurwitz, & Best, 2002) to identify the circumstances that lead to collapsed liquid film. Assuming solid body rotation, Samsonov (1971) found that critical Weber number that causes experiencing liquid film breakdown depends on the aspect ratio of H/R_i as described in Chapter 5.

It is worth mentioning that even though Samsonov attributes the instability entirely to the force imbalance at the interface but his case does not have moving free surface (radially-fixed interface). Such cases are usually studied by linear hydrodynamic stability theory. One cause of instability in this theory is the surge of capillary force versus the centrifugal force at the interface which amplifies the added perturbation to end up to breakdown (Bandyopadhyay, & Gad-el-Hak, 1996). The perturbation takes a form of a complex exponential function that is considered as a sinusoidal wave-like with a spatial and temporal factors of wavenumber and frequency. The perturbation is plugged into the

governing equations of motion at stable condition to develop a disturbance in the flow field which determines the criteria for the interface instability. In the case of a swirling flow in microgravity environment, applying this approach gives formulas that contain wavenumbers and frequencies due to the inclusion of perturbation modes as well as Weber number due to performing stress balance at the interface (Weidman, Goto, & Fridberg, 1997). Since in the present problem we are analyzing the free surface motion in the separator, the surface is no longer purely cylindrical and the liquid is in a complex motion, not just in sold-body rotation. The free surface simply collapses as the surface tension effects overcomes the centrifugal force. Since the problem in the current work involves a moving free surface (dynamic boundary), a different approach is needed to understand the reason and the circumstances that develop liquid film collapse. This study utilizes the CWRU separator mentioned earlier to conduct the stability investigation. The next section introduces this separator which is previously presented in several studies (Hoyt, Kang, Kharraz, Kadambi, & Kamotani, 2011; Kang, Hoyt, Kadambi, & Kamotani, 2014).

1.4 CWRU Separator

As mentioned earlier the separator is an updated version of the CSD-C NASA design. The separator is shown in Figure 1.1 which has a general appearance of a cylindrical compartment that is divided into two parts using what is called baffle plate. The part above the baffle plate is where the separation process takes place by injecting the flow through an inlet nozzle to develop a swirling flow with centrifugal force that induces the

medium to be segregated into liquid film that coats the separator wall and gas core which extends axially along the separator up to the baffle plate. The purpose of the baffle plate mainly is to maintain the arrangement of the gas core and liquid film. This part also contains the gas outlet which releases the separated gas. After separation the liquid moves to the lower part through a gap between the baffle plate and the separator walls. The pressure in the liquid film increases towards the separator wall. Since the gap is relatively small compared to the liquid film, only the liquid near the wall can move through the gap, so the removed liquid is under high pressure.

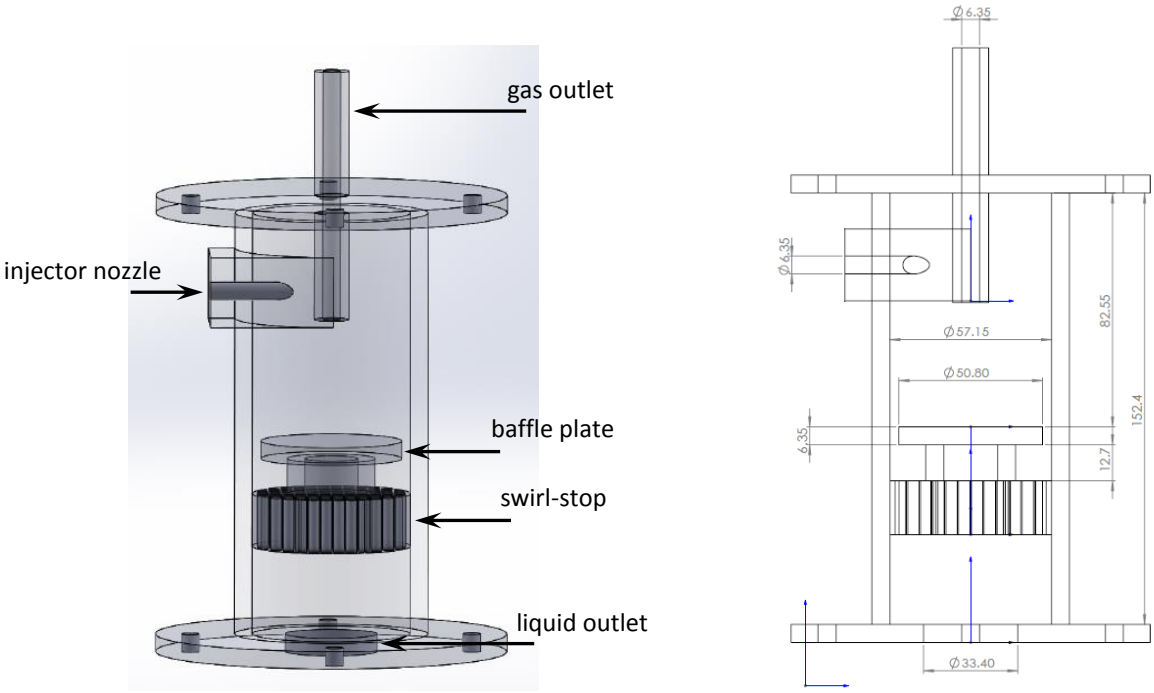

Fig. 1.1 Cyclone separator geometry used in this study: (a) schematic and (b) pertinent dimensions (in mm)

The lower part contains a swirl-stop (honeycomb) to suppress the swirl, which makes it possible to remove the liquid from the liquid outlet. The liquid phase leaves the separator at the bottom center. The liquid is eventually discharged into atmosphere. To decrease the liquid gage pressure to zero, a backpressure valve is situated at the liquid outlet line. During the operation, the valve opening is adjusted to balance the pressure build-up in the liquid film in the separator. The baffle plate location can be adjusted to provide the upper part with a range of aspect ratio (length/diameter).

1.5 Significance of the Study

Going to space to conduct mission exploration or launching research laboratory into orbit such as the International Space Station, ISS, requires full understanding of the behavior of substance in the absence of gravity. In liquid flow applications, this environment features strong presence of capillary force. The effect of this force is very pronounced in flows with free surfaces. Therefore, cyclonic separators are highly entitled for the need of sufficient investigation due to the presence of free surface in this case. As explained earlier, the tangential injection of the flow produces swirl flow inside the separator housing with angular momentum that creates increased centrifugal force in the radial direction. The results is a configuration of gas core along the separator axis and liquid film coating the separator walls. It is important to maintain this flow field configuration in order for the separation process to happen and continue. Achieving this task can be analytically performed by the use of conservation of angular momentum and pressure balance. The pressures that need to be balanced in this case are pressure created by the

centrifugal force, pressure due to the effect of surface tension at the interface, and back pressure caused by the presence of a valve at the liquid outlet. Any imbalance between those pressures leads to variation (decrease or increase) in the liquid film thickness to regain the balance. If the liquid film increased to become quite thick, the capillary force influence at the interface becomes high to a point that eventually may lead to liquid film collapsing. This end is indeed not desirable particularly in space applications where adjusting operating conditions to obtain proper separation condition is not always accessible. To prevent such collapsing, therefore, certain arrangements need to be implemented and that requires a good understanding to the fluid physics of the swirling flow inside cyclonic separators. Once the nature of the problem is understood, mathematical formulas as well as computational models can be used to predict the initiation of collapsing. The experimental approach in this case however, involves technical setbacks that complicate its use to study this aspect. Providing microgravity environment for sufficient time is one costly task to conduct experiments. Drop towers and aircraft parabola flights are not capable to provide sufficient time to reach steady state in cyclonic separators reduced gravity experiments (Hoyt, Kang, Kharraz, Kadambi, & Kamotani, 2012). Going to space to conduct complete experiments that cover transient and steady state cases requires a lot of time and expenditures. In this case, it is reasonable to use computational methods which recently have shown satisfactory results in the analysis and design of applications in industry and engineering applications. This work utilizes this approach to analyze and investigate the circumstances and the causes that lead to develop unstable liquid film inside the CWRU passive cyclonic separator in zero

gravity environment. Also, control-volume approximation is utilized to provide primary insight into the physics of the problem.

1.6 Objectives

This study is intended to understand the effect of surface tension on the swirling flow inside passive cyclonic separators in microgravity environment in case of liquid-only injection and achieves the following,

1. Addressing the effect of separator geometry and the flow field hydrodynamics on the behavior of the swirling flow by conducting parametric study.
2. Clarifying the cause and the circumstances that lead to the event of liquid film collapsing in order to establish a criteria that predicts the inception of this event.

Analytical and computational approaches are used to achieve the above objectives. Liquid- only injection case is mainly investigated.

Chapter 2 Literature Review

Swirling flow is a one common flow that is very present in industry and engineering applications. Oil industry recently started to use cyclonic separators in refining processes to purify the produced oil from undesirable liquids and solids as well as extracting natural gas using this process (Wang, Gomez, Mohan, Shoham, & Kouba, 2003). In the combustion process, swirling jets are utilized to obtain a stable flame and increase the efficiency of mixing (Huang & Yang, 2005). The wide spread use of this type of flow demands the need of good understanding of the fluid physics that explains the flow field behavior. Towards that end, a large amount of study has been carried out covering mostly all aspects related to science and engineering. One major and important field in the study of swirling flow addresses the stability of the flow field considering the causes and the circumstances that lead to an improper flow field configuration inside cyclonic separators. Computational and experimental approaches are utilized to investigate this concern. This chapter reviews those efforts with more emphasis on swirling flow inside passive cyclonic separators.

2.1 Hydrodynamic Stability

A vast amount of research has been conducted utilizing the hydrodynamic stability to investigate many fluid flow instability. This approach basically probes a disturbance which is theoretically added to a stable flow field to predict the circumstances that lead to unstable flow fields. This disturbance is a form of temporal and spatial exponential function with constants that represent the frequency and the wavenumber respectively.

The growth of perturbation leads to an unstable case while its decay produces a stable flow field. The stability of rotational flow associated with free surface in a zero gravity environment is one classical subject that came under extensive investigation utilizing the hydrodynamic stability theory to explain the fate of unstable condition.

The first step in this field of study was taken by Rayleigh (Rayleigh, 1879). He established criterion for the stability of inviscid swirl flow with free surface proposing that this flow is stable to axisymmetric infinitesimal perturbation if and only if the magnitude of the circulation increases in the radial direction that is perpendicular to the axis of the rotation. In mathematical form it is

$$\phi(r) = \frac{1}{r^3}\frac{d}{dr}\left(r^2 u_\theta^2\right) \geq 0 \qquad \text{(EQU 2.1)}$$

In later work, Rayleigh (1892) introduced a study taking into account the effect of surface tension on cylindrical surfaces. His investigation proposed a non-rotational cylindrical inviscid liquid column under a symmetrical perturbation of wave length λ and frequency q. Rayleigh specified that, the liquid column reaches instability if the wave length exceeds the circumference, $2\pi a$, of the cylinder cross section where a is the cross section radius.

For rotating flow, Taylor (1923) investigated theoretically and experimentally the swirling flow between two rotating coaxial cylinders with radii R_1 and R_2. The two cylinders were rotated with angular velocities of ω_1 and ω_2 to develop swirl flow. Taylor made some assumptions to simplify the problem considering that the flow can be treated as Couette flow. Proposing a normal mode to create the perturbation, he applied linear stability

theory ending up to solve Bessel functions. The solution was in very close agreement with his experimental results including both cases of axisymmetric and non-axisymmetric perturbations. Using Rayleigh criterion, Taylor concluded that the stability can be achieved if and only if the outer cylinder has circulation greater than the inner one $(\omega_2 R_2^2 > \omega_1 R_1^2)$ and both are in same direction of rotation.

The role of surface tension on the stability of rotational flow with free surface is found critical also in the rotational flow of liquid columns. As mentioned above, the early work in this field was by Rayleigh but adding rotation to the flow field was first introduced by Hocking and Michael (1959) proposing that an inviscid liquid column spins rigidly (solid body rotation) at angular velocity ω. They found for azimuthal (planar) disturbances the stability can be attained if $\frac{\sigma}{\rho a^3 \omega^2} \geq \frac{1}{m(m+1)}$. The ratio $\frac{\sigma}{\rho a^3 \omega^2}$ is in fact the inverse of Weber number which later named by Weidman (1994) as Hocking parameter. For all wave numbers, the authors postulated that the liquid column is stable if Hocking parameter is $> \frac{1}{6}$. At a certain wave number it is obvious that the increase of surface tension carries more stability to the flow field.

Rotational flow in some cases involves an inner free surface such as the case of this study where a gas core extends axially along the separator and radially outward to meet the liquid film and forms free surface. The effect of this free surface on the stability of rotating flow was the case of interest in Pedley and Michael (1967) work. Their work considered two types of inviscid rotating flow configurations describing the first as a liquid column

with flow boundaries at radii $r = 0$ and $r = a$ and the second with $r = a$ and $r = \infty$ which can be identified as gas core in unbounded liquid film. The authors generalized their work by providing azimuthal velocity in terms of the radius, $u_\theta(r)$, that is neither restricted to vortex flow $\left(u_\theta \propto \frac{1}{r}\right)$ nor solid body rotation flow $(u_\theta \propto r)$. Pedley and Michael (1967) argued that two types of stability conditions are required in order to ensure a full stable flow field. The first one requires fulfilling Rayleigh criterion of the outward increase of the circulation specified in Equation 2.1. The second stability condition is specified by them in a form of an equation which can be used in the case when the free surface is the outer boundary of the flow (liquid column), and also for the case when the free surface is the inner boundary of the flow.

For rotating flow of two different fluids inside cylinder, Weidman and his co-workers (Weidman, 1994; Weidman, Goto, & Fridberg, 1997) conducted a comprehensive analysis of two rotating immiscible fluids subject to axisymmetric, planar, and spiral perturbations for both cases of inviscid and viscous flow and a stability criterion is analytically derived.

It is obvious that linear stability theory of rotating flow with free surfaces addresses flow domains with radially-fixed interface boundary and any instability encountered is due to a growth of added disturbances to eventually cause chaotic flow field. In comparison, the instability experienced in this study is created by a mechanism that is different from the one described above. In cyclonic separators in microgravity environment, instability is encountered due to unbalanced forces affecting the liquid film at the interface which

characterizes moving behavior. The coming literature addresses in general the cyclonic separators with focus on the circumstances that yield liquid film collapse or undesirable rotating configuration.

2.2 Stability of Swirling Flow in Cyclonic Separators

Proper flow configuration is important to perform efficient separation which requires avoiding consequences that lead to liquid film collapsing. As mentioned earlier, in flow field with moving boundary the unbalanced forces causes instability. In microgravity environment in cyclonic separators, these forces are mainly the centrifugal force created by the angular momentum of the rotating flow and the capillary force due to surface tension effect at the interface.

Other kinds of undesirable flow configuration in cyclonic separators involves waviness and tapering in the gas core due to high length to diameter ratio (Hoffmann & Stein, 2008). This situation is studied by Bandyopadhyay and Gad-el-Hak (1996) for passive cyclonic separator in normal gravity. The gas core behavior while changing the length-to-diameter ratio (aspect ratio, L/D) and the tangential relative angle between the inlet and the outlet (Φ) are experimentally studied. Based on direct observations using a high speed camera, the study categorized the gas core configuration mainly into straight and spiral-helical modes but several other modes can develop from the combination of those two main modes. The authors introduced a configuration map in terms of L/D versus Φ describing all of the possible configuration modes in regions that are demarcated using

parallel lines named as π-lines. The study pointed out that the optimum and preferred gas core modes are those with straightening configurations which enhances the separation efficiency as a result of aligning the gas outlet with the gas core. These optimum modes are illustrated on the configuration map along with its π-lines. Also, it is found that the inlet volume flow rate showed insignificant influence on the gas core behavior as long as the gas volume fraction is kept constant. Unstable gas core configurations are noticed to happen at large aspect ratios. The study presented simple kinematic model relating the gas core radius to the inlet-outlet angle, Φ. The instability part in the author's work concerns the instability of the gas core configuration due to the presence of waviness and tapering which affects the gas core alignment with the gas outlet. Also for a high aspect ratio, the lower end of the gas core becomes weakly attached to the wall and starts to move (precess). This kind of instability is different from the current work where the whole interface experiences radial and inward movement due to unbalanced forces.

The gas core configuration is also important in bubble separation. Ahn, et al. (2000) found that the size of the gas core affects the separation efficiency of bubbles. Under microgravity environment, the study utilized two kinds of centrifugal separators, A and B, as shown in Figure 2.1 to investigate the parameters that determine the time for the bubble to transfer to the gas side. In the first kind (separator A), the two-phase flow is injected through a looped tube where the centrifugal force separates the flow into a liquid

layer that stratifies touching the upper tube wall and a gas layer that accumulates flowing on the lower tube wall.

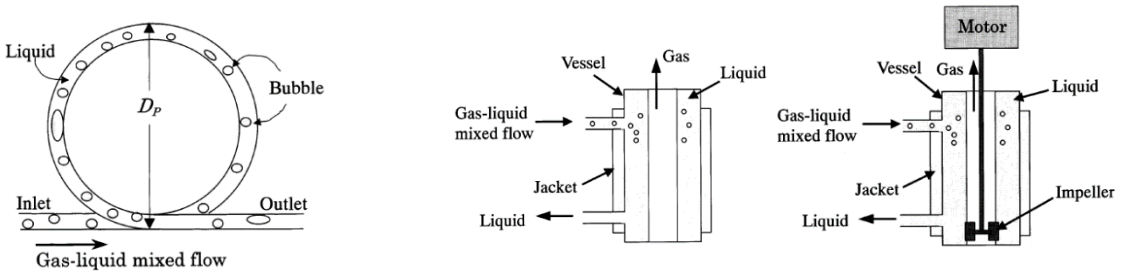

separator A separator B

Fig. 2.1 Schematic diagram of the separators used by Ahn et al. (figure from Ahn, et al., 2000)

The second kind (separator B) is a cyclonic separator where the two-phase flow is separated inside a cylindrical compartment by the virtue of centrifugal force. The centrifugal force in this separator is created using two techniques: injecting the flow tangentially through the inlet (passive method), and agitating the flow using an impeller located at the bottom of the separator (active method). For separator A, the study showed theoretically that decreasing the tube diameter enhances the bubble separation as the bubble time transfer decreases. It is also shown that the efficiency of bubble separation in separator B increases with the increase of the gas core volume which can be achieved through higher inlet flow velocity. This is using the first technique (passive method) while for the second technique (active method) it can be enhanced through increasing the agitation speed. Smaller bubbles are more difficult to separate than the bigger ones for both separators.

The liquid film collapse in cyclonic separators due to unbalanced forces mentioned earlier is studied by Bean, et al. (2002). Using passive cyclonic separator developed in the Interphase Transport Phenomena (ITP) laboratory at Texas A&M University (TAMU), the study carried out a microgravity experiment on NASA's KC-135 aircraft. The separator is basically similar in design to the CWRU separator described earlier. The two-phase flow is injected through a nozzle located in the middle of the separator housing where the swirling flow is developed. The inertia difference between the two phases of the swirling flow creates configuration of a gas core surrounded by a liquid film. A baffle plate located at the bottom of the separator delimits the extent of this configuration as beyond this barrier only liquid phase accumulates and exits to its outlet. The gas phase is released through a pipe that extends axially from the separator top. Four days of parabolic flights were performed to collect reduced gravity data as for each day a range of inlet flow rates were used at four cases of gas core diameter. The gas core diameter in each case is determined from a starting liquid volume in normal gravity as $D_I = D[1 - (h/L)]^{1/2}$. The force balance between the centrifugal force and the capillary force identified by Weber number at the interface was used to investigate the behavior of the swirling flow configuration. Assuming solid body rotation, the angular velocity, ω, is obtained from the inlet flow rate and plotted against the gas core diameter as depicted in Figure 2.2 to show the liquid film stability regions with boundaries defined by Weber number. The authors introduced the term "necking" which represents the liquid film collapsing in situations with thick liquid film to a point where it bridges the gas core and forms discontinuous gas regions.

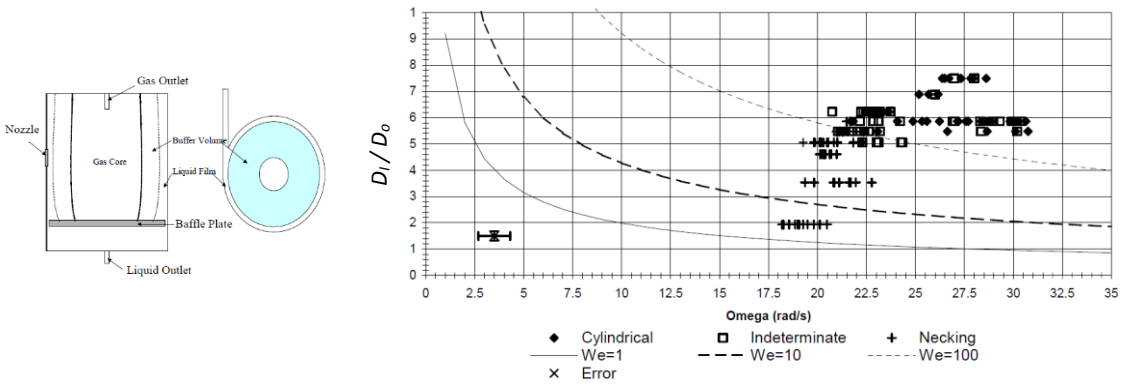

Fig. 2.2 Regions of critical Weber number of Bean et al. results (figure from Bean, et al., 2002)

As shown in Figure 2.2, to avoid necking, the study results found that interfacial Weber number of two or larger is required implying that the centrifugal force must be twice or more than the capillary force. The results also showed that proper swirling flow configuration and optimum gas core formation require Weber number larger than 100.

The ability of passive cyclonic separators to change the liquid film thickness gives these devices the advantage to work on a wide range of inlet flow rates, however; once the liquid film evolves to an exceedingly thick layer, the worry about efficient bubble separation arises to a serious concern referring to the fact that more time is required for bubbles to reach the gas core. As a consequence of this complication, the separator may experience what is called a carry-under where bubbles encroach into the liquid outlet. Thick liquid film in microgravity environment in particular may also end up causing collapse due to the rise of capillary force over other adverse forces such as the centrifugal force and at extreme cases the liquid phase floods the gas outlet which is a case of what is called carry-over. To avoid such an event, it is important to establish a proper swirling

flow configuration. In this regard, Ellis, et al. (2005) and Ellis, et al. (2006) investigated the intrinsic parameters of swirling flow inside a passive cyclonic separator aiming to optimize the design to enhance the separation performance through studying the bubble dynamics of the incoming gas phase and the gas core behavior. For this objective, the TAMU passive cyclonic separator is employed to conduct ground-based and microgravity experiments aboard the NASA KC-135 aircraft. In addition, an analytical approach and CFD modeling were employed to reach simple a quantitative expression that gives physical insight into the problem. The study investigated the effect of volume flow rate, separator diameter and injection nozzle area on the tangential velocity as this later quantity determines the amount of swirling flow angular momentum which creates the gravitational-like field to perform separation. This velocity also dictates the gas core radius value which is critical for the bubble separation mechanism. The results depict that tangential velocity has direct proportionality with the flow rate while inverse proportionality is shown for this velocity against the separator diameter and the injection nozzle area. The CFD data were in good agreement with the experimental results. Their analytical approach utilized the force balance between buoyancy and drag forces that affect the bubble movement to predict the radial and the axial bubble transit time assuming that the bubble travels at its terminal velocity. The radial transit time represents the time required for the bubble to coalesce in the gas core while the axial transit time is defined as the time taken by the bubble to travel from the injection region to the liquid outlet. The study calculations show a rapid decrease in the ratio of radial to axial transit

time as the gas core increases. Also similar behavior for this ratio is shown when the volume flow rate increases.

Space power generation using thermal power cycles involves two-phase flow which is not desirable in some stages such as having moisture in the vapor delivered to the turbine. With the very high velocity associated with the working fluid flowing to the turbine, any liquid droplets accompanied will cause severe erosion to the turbine blades in the long run. One way to prevent these complications is to utilize a phase separation device such as a cyclonic separator at the turbine inlet to perform the separation and ensure that only vapor is delivered. A work was introduced by Supak (2007) addressed the use of this technique through an experimental study in microgravity environment. NASA C-9 reduced gravity aircraft is used to perform parabolic flights as liquid-metal Rankine cycle equipped with passive cyclonic separators was operated on board to investigate the power cycle performance. The separators are aimed to replace other components such as radiators and heat exchangers claiming that this alteration enhances the power cycle performance. The separators used are similar to the passive cyclonic separator used by Bean, et al. (2002) mentioned earlier. The experiment is conducted by the Interphase Transport Phenomena (ITP) laboratory at Texas A&M University where reduced gravity data is collected for four days from a Rankine power conversion system over a range of single and two-phase mass flow rate. An analysis is performed to this data investigating the effect of integrating cyclonic separators on Rankine cycle performance and mass as a sizing model is developed to predict the optimum separator mass while taking into

account the hydrodynamic parameters and the behavior of the swirling flow field inside the separator. The work of Supak (2007) investigated also the criteria to maintain proper swirl configuration by applying force balance at the interface between the centrifugal force and the capillary force which is identified by the dimensionless quantity of interfacial Weber number. It is found that proper swirl configuration requires an interfacial Weber number equals to 100 which is the same value introduced by Bean, et al. (2002).

Since capillary force plays a major role in flow field behavior in space, researches turn to exploit this feature in designing phase separation devices for space use. In a development process of several stages, Thomas, et al. (2008) and Weislogel, et al. (2008) constructed a phase separator based on the capillary action of liquids. The device is proposed to replace rotary separators in the NASA space mission for urine collection. Their separator utilizes a passive technique relying upon the wetting characteristic (determined by the contact angle) of the liquid phase and the capillary pressure drop across a meniscus interface. The separator is simply a helix (spiral conduit) with a cross-sectional area of an ice-cream-cone shape and this area increases gradually as the helix advances to eventually form a space that works as a collector to the segregated phases. To enhance wetting, the conduit is provided by vanes that go along the wedge angle. The injected liquid phase creates a meniscus around the ice-cream-cone angle (wedge angle). The capillary action at the wedge and the capillary pressure at the meniscus interface retain a similar meniscus shape and any extra coming liquid is sent along the wedge angle to form a continuous

liquid phase stream (rivulet) which is eventually collected through liquid drain and the gas phase is vented. The design utilizes also the centrifugal force of the incoming flow to coalesce liquid droplets into the rivulet. The final separator design is reached after six stages of designing attempts as reduced gravity experiments were carried out on NASA's C-9 aircraft to test each design. To maintain proper flow configuration and hold the liquid stream adhered to the wall, the study proposed Weber number to be larger than 3 to ensure stable flow. Even though the study presented novel separator design based on a simple approach but the separator demonstrated deficiency in reaching total gas and liquid separation. Also the design can handle only low flow rates.

TAMU and CWRU phase separators have limited ability to work efficiently at very low void fraction. DYNAFLOW, INC. developed a separator that basically utilizes passive approach to handle void fraction to a values as low as 0.01%. The work is introduced by Wu and Chahine (2012) as part of an inclusive project supported by NASA to study phase separation in microgravity environment which covers low and high void fraction. The separator operates typically at large liquid inventory which consequently yields very small diameter gas core. This configuration makes it difficult to maintain a stable and continuous gas core. However, their design demonstrated good performance in constructing a steady and persistent gas core that was able to succeed in making operational separator. The study presented an analytical equation as a criterion to establish stable gas thread and provide continuous separation. A reduced gravity experiment that was carried out as NASA Boeing 727 aircraft was employed to perform

several parabola flights. Computational work was also performed using self-developed software which aimed to handle both the dispersed bubbles and free surfaces. The experimental results showed that the separator was successfully able to establish and maintain a stable gas thread. In addition, the separator achieved a remarkable level of separation as the void fraction reduced from 10^{-2} to 10^{-8}. The authors utilized CFD computations to assist in designing the separator to optimize the performance while taking into consideration the bubble dynamics effect.

2.3 Two-Phase Flow Separator Experiment (TPFSE) Project

The project is an extensive research program supported by NASA to perform a comprehensive assessment for the aim of utilizing passive cyclonic separators in spacecraft systems as ground-based and microgravity experimentation were carried out to figure out the performance and the range of operability of such devices. In 1990, Glenn Research Center started work on developing passive cyclonic separator that accomplishes the desired task to end up to a design named as the Cascade Cyclonic Separation Device (CSD-C) (Hoyt, 2007; Hoyt, Kamotani, Kadambi, McQuillen, & Sankovic, 2008). This design in fact is just the pre-version of CWRU separator as it uses the similar passive separation technique of utilizing the angular momentum of the injected flow to develop a centrifugal force which creates the arrangement of a gas core surrounded by a liquid film. Hoyt, et al. (2008) utilized the CSD-C separator to perform computational work investigating the operation modes and analyzing design modifications to enhance the separator performance. Euler-Euler approach is utilized to perform a CFD simulation with

considering the force exchange between the two phases. The authors described four flow modes (flow configurations) that typically represent the cases of operation inside the separator. The efficacy of the separator is also evaluated by comparing the removed liquid and gas volumetric flow rates at the respective outlets to the inlet liquid and gas volumetric flow rates respectively. The study concluded that design modifications to the outlets allows the separator to work on a wider range of performance.

After a few years of Hoyt, et al. (2008) work, a modified version of CSD-C separator is designed at CWRU to conduct extensive work investigating experimentally and computationally the range of operability and the physics phenomena that govern the steady and transient states. The design and the mechanism of the separator is previously detailed in Chapter 1. Hoyt, et al. (2011) utilized experimental, computational and analytical approaches to quantitatively evaluate the behavior of the CWRU separator for steady and transient conditions. Their experiment is carried out at relatively high flow rate range due to the need of a sufficient rotation to overcome the gravity effect and prevent collapsing (achieving high Froude number). The study derived an analytical formula that predicts the liquid annulus thickness through applying a pressure balance between the developed pressure due to the rotational flow and the pressures at the outlets of the gas and liquid phases. The dynamic response of the separator to transient flow was also investigated. It is shown that the separator can efficiently handle varied injection flow rates by the virtue of the pressure balance mentioned above which

consequently causes variation in the gas core radius (liquid annulus thickness) to accommodate the pressure changes.

To gain more insight into the transient behavior of the CWRU separator, Hoyt, et al. (2012) investigated the dynamic response of this device via applying step-changes to the inlet volume flow rate for single and multiphase flow. Experimental, numerical and analytical approaches were employed to achieve the task. The computational modeling is developed utilizing a hybrid CFD solver that combines Euler-Euler multiphase approach with phase-field interface method. The study used the separator housing that contains the configuration of gas core and liquid annulus as a control volume to impose the conservation of mass and angular momentum along with applying a pressure balance to develop analytical model that describes the transient behavior of the separator. The results of the three approaches of experimental, CFD and analytical were presented showing acceptable agreement. The steady state gas core radius versus the inlet flow rate is predicted using CFD and control-volume approximation.

In a follow-up study to reach further understanding to the physical phenomena that characterize the CWRU separator, Hoyt, et al. (2013) presented an inclusive work investigating the steady and transient states of this separator by means of experimentation, CFD and analytic approaches. In their experiment, a device that utilizes electric resistivity principle is used to measure the gas core radius. This device which is called electric resistance tomography (ERT) system is tooled up with several sensors

which are installed at equal distances surrounding the separator periphery to read the electrical resistivity distribution. The study develops a CFD solver that integrates VOF method which is highly efficient in capturing free surfaces with the Euler-Euler method to come up with a hybrid code that can concurrently treat the dual presence of dispersed phase and interface. The experimental and CFD results of the gas core radius show acceptable agreement. For swirling flow in separators, the skin friction coefficient is critical in determining the liquid annulus thickness, therefor the authors develop a correlation to estimate this quantity in terms of Reynolds number. The steady state for two-phase flow was studied investigating the effect of gas volumetric quality, β, on the gas core radius.

Since the CWRU separator is intended to be used in space, Hoyt (2013) conducted a reduced gravity experiment for the sake of validating the CFD and control-volume approximation results. In a program managed and supported by NASA, a parabolic flights aboard Zero-G Corporation Boeing 727 was utilized to produce reduced gravity environment to carry out the experiment. The test section used is a passive cyclonic separator that has similar shape and design as the CWRU separator mentioned earlier but with slightly larger size. The reduced gravity period in parabolic flights is limited and as the injection volume flow rate decreases, more time is needed to reach steady state. As a consequence, the author was not able to execute low injection flow rates which is needed to capture the surface tension effect and the lowest injection flow rate that was achieved was 4 LPM.

Kang, et al. (2014) introduced an extension work to what Hoyt, et al. (2013) have started where this time they investigated the hydrodynamic development and variations of the separator flow field in case of two-phase flow injection. The study mostly focused on the variation of the gas core radius concluding that all variations are related to the wall friction. The methods of research used by Hoyt, et al. (2013) of experimental, theoretical and CFD approaches, are also followed by the authors to address the problem. Electric resistance tomography (ERT) was used to configure the gas core radius. The CFD methodology employed the solver that was discussed earlier in Hoyt, et al. (2013). It is a hybrid code of VOF and Euler-Euler methods which is previously mentioned as able to simulate dispersed bubbly flow associated with free surface. Referring to Hoyt, et al. (2013) of achieving satisfactory results using 2-D axisymmetric mesh, the authors utilized similar model to simulate the separator. One further achievement in Kang, et al. (2014) work was introducing control volume model that describes two-phase flow injection.

Another aspect that is investigated in Kang, et al. (2014) work concerning the effect of inlet nozzle size on the gas core radius in two-phase flow injection. The study also found that the $\alpha - \beta$ relationship significantly influences the separator behavior. The case when $\alpha \neq \beta$ which is referred to as inhomogeneous flow is experimentally observed in small length to diameter ratio, L_N/D_N, of the nozzle and to establish homogeneous flow (i.e. $\alpha = \beta$), this ratio must be larger than 10. The results show that nozzles with inhomogeneous flow (i.e. $L_N/D_N < 10$) affects the gas core radius at given β but no

effect is observed for nozzles with homogeneous flow (i.e. $L_N/D_N \geq 10$). For CFD simulation, the flow in the nozzle was assumed homogeneous as no credible correlation can reasonably describe the $\alpha - \beta$ relationship inside nozzles.

Chapter 3 Analytical Description

The flow behavior inside the separator can be phenomenologically described in simple manner by making reasonable assumption to develop a mathematical model that explains the physics of the problem. Such methodology provides a primary insight that allows for some perspective and prediction of the outcome. Also it does not require as much computations and time as in the CFD approach to obtain results. This methodology is implemented using control-volume approximation. Since this study concerns a low injection flow rate in microgravity environment, the effect of surface tension at the interface is very important in this case. This effect of surface tension is explicitly related to the interface curvature. The following section introduces the role of interface curvature in the analysis of surface tension which is required in order to specify the appropriate radius curvature for this study.

3.1 Radius of Curvature

The presence of a free surface (interface) in this study implies significant role for the radius of curvature in swirling flow hydrodynamics. In surface tension analysis, there are two radii of curvature as shown in Figure 3.1. The pressure difference across the interface can be obtain using Young-Laplace equation as

$$\Delta p = -\sigma\left(\frac{1}{R_1}+\frac{1}{R_2}\right)=\frac{\sigma}{R_i} \qquad \text{(EQU 3.1)}$$

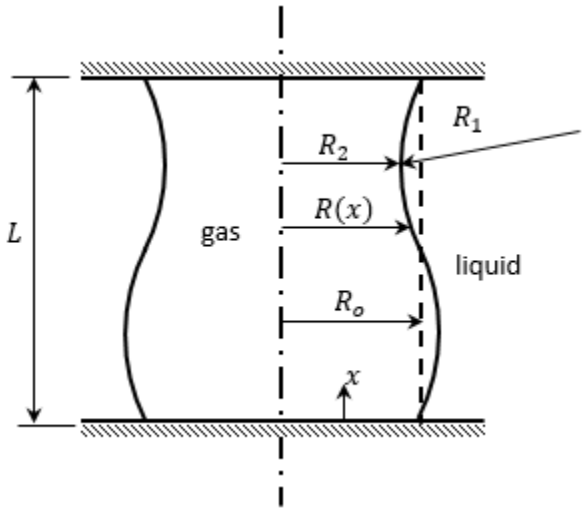

Fig. 3.1 Radii of curvature for gas-liquid interface

The radii of curvatures, R_1 and R_2 can be expressed mathematically as

$$\frac{1}{R_1} = \frac{-d^2R/dx^2}{[1+(dR/dx)^2]^{3/2}} \qquad \text{(EQU 3.2)}$$

$$\frac{1}{R_2} = \frac{1}{R[1+(dR/dx)^2]^{1/2}} \qquad \text{(EQU 3.3)}$$

In order to determine the significance of each parameter in the above equations, a scaling analysis is carried out by non-dimensionalizing the two equations with characteristic lengths of R_o and L. Thus, the dimensionless parameters are $r = R/R_o$ and $x^* = x/L$ and the above equation will be

$$\frac{1}{r_1} = \frac{-\frac{R_o^2}{L^2}\frac{d^2r}{dx^{*2}}}{\left[1+\frac{R_o^2}{L^2}\left(\frac{dr}{dx^*}\right)^2\right]^{3/2}} \qquad \text{(EQU 3.4)}$$

$$\frac{1}{r_2} = \frac{1}{r\left[1+\frac{R_o^2}{L^2}\left(\frac{dr}{dx^*}\right)^2\right]^{1/2}} \qquad \text{(EQU 3.5)}$$

It is clear that the aspect ratio of R_o/L determines the significance of each radius of curvature. For unit-order aspect ratio $(L \approx R_o)$, both radii are important. For a high aspect ratio $(L \gg R_o)$, Equation 3.4 shows that r_1 is large (cylindrical interface configuration). According to the Young-Laplace equation, this implies a smaller contribution of this radius of curvature to the pressure drop, so that r_2 becomes significant in this case. A low aspect ratio $(L \ll R_o)$ is not considered in the present separator work.

In the control-volume analysis discussed below, the free surface shape is assumed to be a right circular cylinder, for simplicity. In this case, $R_1 = \infty$ and $R_2 = R_0$. From the above discussion, this approximation is true when the aspect ratio is large.

3.2 Control-Volume Approximation

This approach is one of two methods used in this study to investigate and analyze the flow development and hydrodynamics inside the separator. The control-volume approximation utilizes mass conservation, the conservation of angular momentum and the pressure balance on the liquid film to obtain non-dimensional parameters that affect the liquid film behavior. As shown in Figure 3.2, the respective control volume considers only the separation housing where the configuration of gas core and liquid annulus occurs and the separation process takes place. In this study the liquid-only injection is considered.

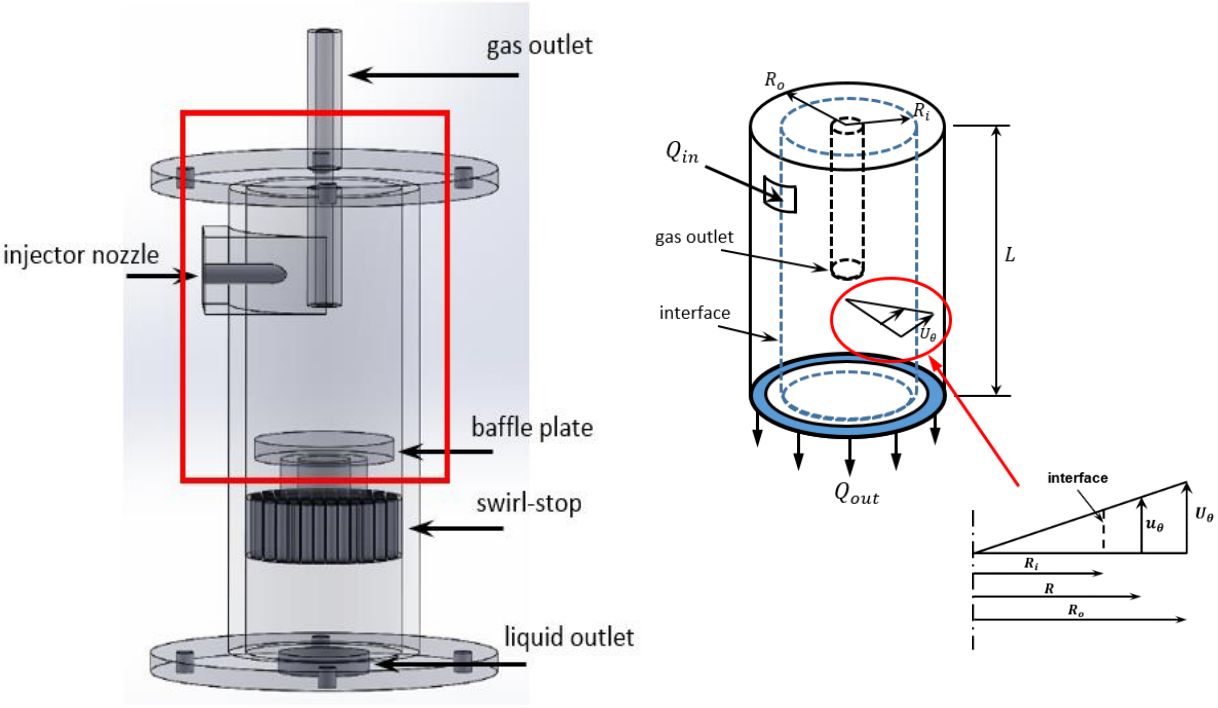

Fig. 3.2 Computational domain of the control-volume approximation

Since the formed liquid film is assumed to have a uniform annulus shape, the mass balance (conservation of mass) gives,

$$\rho Q_{in} = \rho Q_{out} + \frac{d[\rho L(\pi R_o^2 - \pi R_i^2)]}{dt} \qquad \text{(EQU 3.6)}$$

Therefore, the continuity equation that described the separator mass balance can be written as

$$Q_{in} = Q_{out} - \pi L \frac{d(R_i^2)}{dt} \qquad \text{(EQU 3.7)}$$

Applying the conservation of angular momentum, the angular momentum flux of the flow that enters the separator is equivalent to the rate of change of liquid film angular

momentum, the angular momentum flux that leaves the separator through the liquid outlet, and the moment of the shear force at the wall due to friction.

$$J_{in} = \frac{dJ_{film}}{dt} + J_{out} + M_{wall} \quad \text{(EQU 3.8)}$$

Using the profile of solid body rotation shown in Figure 3.2, and assuming the liquid outlet is narrow, the average liquid velocity that delivers the angular momentum flux at the liquid outlet can be considered the same as the liquid velocity near the wall, U_θ. This produces flux angular momentum of $J_{out} = R_o \rho Q_{out} U_\theta$. The shear stress at the wall can be expressed as $\tau_w = (1/2)\rho U_\theta^2 C_f$ where C_f is the skin friction coefficient. Therefore, the angular momentum due to wall shear force can be obtained in terms of the skin friction coefficient of C_f as $M_{wall} = \tau_w A_w R_o = \pi R_o^2 L \rho U_\theta^2 C_f$. The injected volume flow rate, $Q_{in} = A_{inj} U_{in}$, carries an angular momentum flux of $J_{in} = \rho R_o Q_{in} U_{in} = \rho R_o A_{inj} U_{in}^2$. For linear velocity profile that characterizes solid body rotation that is shown in Figure 3.2, the liquid film angular momentum can be expressed as

$$J_{film} = \int_{R_i}^{R_o} \rho \times (2\pi R \, dR \times L) \times u_\theta \times R \quad \text{(EQU 3.9)}$$

For solid body rotation, $u_\theta = (U_\theta / R_o) R$, thus

$$J_{film} = \frac{2\pi\rho L U_\theta}{R_o} \int_{R_i}^{R_o} \mathrm{R}^3 \, dR \quad \text{(EQU 3.10)}$$

Therefore,

$$J_{film} = \frac{\pi\rho L (R_o^4 - R_i^4) U_\theta}{2R_o} \quad \text{(EQU 3.11)}$$

The presence of a valve at the liquid outlet with backpressure coefficient, K, creates pressure loss that confines the liquid film from passing to the outside. This elevates the

pressure above the baffle plate and the liquid film expands to accommodate the situation. However, the pressure build up due to the centrifugal force opposes this action by pushing the liquid film toward the separator walls. This mechanism describes the pressure balance that occurs in normal gravity. In microgravity environment, the influence of surface tension arises to an extent that needs to be taken into consideration. The surface tension effect in this case appears as a pressure jump across the interface which an mentioned earlier can be expressed as σ/R_i. The dynamics of the liquid film behavior can be obtained for solid body rotation $(u_\theta = (U_\theta/R_o)R)$ by executing pressure balance which yields the following

$$\int_{R_i}^{R_o} \frac{dp}{dR} dR = \int_{R_i}^{R_o} \frac{\rho u_\theta^2}{R} dR = \frac{\rho U_\theta^2}{2R_o^2}(R_o^2 - R_i^2) = \frac{\sigma}{R_i} + \rho K Q_{out}^2 \qquad \text{(EQU 3.12)}$$

To evaluate the influence of each term in the three governing equations obtained above, a scaling analysis with respect to the injected quantities is performed. The volume flow rate, Q_{in}, the angular momentum, J_{in} , and the dynamic pressure, ρU_{in}, at the inlet are employed as characteristic quantities to scale Equations 3.7, 3.8, and 3.12 respectively. Therefore, these equations can be transformed into dimensionless form as

$$1 = v - \Gamma \frac{dr_i^2}{d\tau} \qquad \text{(EQU 3.13)}$$

$$1 = uv + \frac{\Gamma}{2}\frac{d}{d\tau}\left(u(1 - r_i^4)\right) + \Gamma As C_f u^2 \qquad \text{(EQU 3.14)}$$

$$u^2(1 - r_i^2) = \frac{2}{We_o r_i} + \kappa v^2 \qquad \text{(EQU 3.15)}$$

Dimensionless quantities such as $\Gamma = \pi R_o^2/A_{inj}$, $As = L/R_o$, and $\kappa = 2KA_{inj}^2$ represent the effect of the geometry on the separator behavior. While $r_i = R_i/R_o$, $u = U_\theta/U_{in}$,

$We_o = \rho R_o U_{in}^2/\sigma$, $\nu = Q_{out}/Q_{in}$ and C_f are dynamic quantities that manifest the flow condition inside the separator. τ quantifies the time with respect to the characteristic time scale L/U_{in}.

Using the above three equations, the transient behavior of the separator can be identified. Initially, the pressure difference across the liquid film starts to rise by extending the liquid film thickness. This behavior continues until the outward flow (mass flow rate from the liquid outlet) overcome the accumulated mass in the separator compartment. After some relaxation time the process reaches the steady state and the liquid film stabilizes at final equilibrium thickness. However, in some occasions and due to some circumstances, this equilibrium liquid film cannot maintain and ends to liquid film collapsing. Using the above three derived equations in steady state forms, this study will identify the occasions of experiencing liquid film collapsing, and accordingly finding justification for this incident.

As mentioned in Chapter 2, for swirling flow fields with free surface the interfacial Weber number is used in some literature (Bean, Waghela, Kurwitz, & Best, 2002) as a parameter that predicts the inception of obtaining unacceptable gas core configuration. However, considering this parameter as a measure to predict any disorder in the gas core and liquid film configuration implies that experiencing any instability is related to the interface. This thought of interface instability dependency on Weber number will be clarified later through analyzing the normal stresses at the interface. To investigate whether this

principal is applicable in this study, Equations 3.13, 3.14, and 3.15 which describes the separator flow behavior need to be solved in steady flow condition to determine the critical Weber number for several flow circumstances. The steady flow form of these equations are

$$1 = u + \Gamma A s C_f u^2 \qquad \text{(EQU 3.16)}$$

$$u^2(1 - r_i^2) = \frac{2}{We_o r_i} + \kappa \qquad \text{(EQU 3.17)}$$

Equation 3.13, which represents the continuity equation can be reduced to $v = 1$ for steady state condition. As it will be discussed in Chapter 5, these two steady flow equations are solved simultaneously to obtain the dimensionless variables of u and r_i while We_o is changed to lower values until the critical value of interfacial Weber number, We_i, is reached as when there is no solution that gives real values for u and r_i. As it will be seen in Chapter 5, CFD simulations are carried out to develop a correlations that describes the skin friction coefficient, C_f . This coefficient is described in some literature (Hoyt, Kang, Lee, Kharraz, Kadambi, and Kamotani, 2013) in a form of $C_f = C\left(Re_f\right)^{-n}$. C and n are constants while Re_f is the liquid film Reynolds number which takes the following form

$$Re_f = \frac{\rho U_\theta (R_o - R_i)}{\mu} \qquad \text{(EQU 3.18)}$$

$$= \frac{\rho U_{in} R_o}{\mu} u(1 - r_i) = Re_o u(1 - r_i) \qquad \text{(EQU 3.19)}$$

The interfacial Weber number can be calculated from $We_i = \rho R_i u_{\theta,i}/\sigma$, where $u_{\theta,i} = (R_i/R_o)U_\theta$ is the tangential velocity at the interface. Knowing that $R_i = r_i R_o$ and $U_\theta = uU_{in}$, the interfacial Weber number can be introduced as

$$We_i = \frac{\rho R_o U_{in}^2}{\sigma} r_i^3 u^2 = We_o r_i^3 u^2 \qquad \text{(EQU 3.20)}$$

This Weber number has been chosen to identify the inception of unstable liquid film proposing that any cause of interface disruption is related to the dynamic nature of the problem of having moving free surface. This behavior, however, is mainly due to the unbalancing between the centrifugal and the capillary forces as it will be seen later in Chapter 5.

Chapter 4 CFD Modeling

Since the concern of this study is passive cyclonic separators in microgravity environment, utilizing the experimental approach involves several complications. Space agencies such as NASA and also other researchers employ drop towers and aircraft parabola flights to create such environment. However, these two techniques are unable to provide sufficient time to reach steady state in those devices (Hoyt, Kang, Kharraz, Kadambi, & Kamotani, 2012). The only way to attain a steady state is to go to space and utilize space shuttles which requires high capabilities of finance and technology. Another option which does not involve such complications is the CFD approach. With the enormous advance in the field of numerical analysis, CFD has become extensively used in a wide variety of fluid mechanics applications. The current study adopts this approach to conduct computational analysis to predict the event of liquid film collapsing inside passive cyclonic separators in zero gravity environment. The working fluid is liquid-only water which is injected tangentially through inlet nozzle inside the separator housing to develop a swirling flow with a configuration of liquid film coating the side walls and a gas core extending along the separator axis. Several software packages are designated to solve fluid mechanics problems but few of them are open access. One open source (free source) CFD simulation framework is OpenFOAM (Open source Field Operation And Manipulation) that has a large platform of finite-volume-based solvers for different areas of research including fluid mechanics. OpenFOAM is written with C++ object-oriented programming and contains an extensive library to build executables for solvers and utilities codes. One major advantage of this software package is the ability to modify any

solver to accommodate the problem characteristics as well as implementing completely new solvers. Nevertheless the user needs some knowledge about C++ code syntax and object-oriented programming basics but the most important is comprehending equations, models, and solving algorithms. For pre-processing, OpenFOAM provides meshing utilities to generate structured and unstructured computational grids for simple and complex geometries.

The swirling flow inside passive cyclonic separators characterizes interface presence which requires certain treatment to capture the surface tension effect on liquid film stability. Several techniques are available in literature that are implemented to track the interface of two immiscible fluids. One common methodology that demonstrates success in dealing with such flow arrangements is VOF (Volume of Fluid) method. The current study employs this method to conduct numerical computations to investigate the dynamics of swirling flow field in association with a moving free surface. This method is a solver that is already implemented in OpenFOAM under the name of interFoam.

4.1 Volume of Fluid (VOF) Method

All of the approaches that are used to study free surfaces falls into two categories namely interface tracking (surface fitting) and interface capturing (surface capturing) (So, Hu, & Adams, 2009; Ubbink, 1997).

In the first one, the interface is identified explicitly using massless markers (points) or represented by the mesh itself where several grid surfaces constitutes the interface. Front tracking (Unverdi, & Tryggvason, 1992) and level set (Osher, & Sethian, 1988) are two reliable and robust methods that utilize interface tracking technique. The front tracking method involves the use of a dynamic mesh to accommodate the changing topology but it is constrained to the distance between each two markers which is a significant disadvantage in modeling bubbles coalescence and breakup. The level set method demonstrates weakness in retaining the conservation of mass principle in the case of complex topologies and in the presence of extreme deformation to the flow such as vorticities.

In the second one, the interface capturing approach, the two phases of the flow domain are discriminated according to how much volume each one occupies using massless particles or an indicator function. Two main methods are in this category: the marker and cell (MAC) (Harlow & Welch, 1965) and volume of fluid (VOF) (Hirt & Nichols, 1981) methods. Since the interface in this approach is not explicitly tracked, the boundary between the phases is not sharply identified and the interface, therefore, smears over span of some grid cells which makes this approach affected by the grid resolution. This drawback raised the concern to find a discretization schemes that reduces the interface diffusion. In VOF method, several schemes are developed to enhance the interface resolution which will be discussed later. The share of each phase in certain grid in VOF method is indicated by void fraction, α. The numeric value of this scalar quantity is

determined by solving the continuity equation shown below over the whole computational domain. The void fraction can be one of the following three cases

$$\alpha = \begin{cases} 1 & \text{entirely phase 1} \\ 0 & \text{entirely phase 2} \\ 0 < \alpha < 1 & \text{mix of both (the interface region)} \end{cases} \quad \text{(EQU 4.1)}$$

Assuming the liquid phase has void fraction of α for incompressible flow, the transport equation of α takes the following form

$$\frac{\partial \alpha}{\partial t} + \nabla \cdot (\alpha U) = 0 \quad \text{(EQU 4.2)}$$

The second term in this equation is accounted for the advection term which has a significant influence on the interface depending on the advection scheme used to discretize this term and obtain a sharp interface. There are several schemes that were developed over the years by researchers. The flux-corrected transport scheme is introduced by Boris and Book (1973). It combines the upwind and downwind fluxes in each cell to produce a scheme with no diffusiveness and instability which are usually associated with the individual use of upwind or downwind scheme (Gopala & van Wachem, 2008). Other different approach identifies the interface using what is called line technique. The SLIC (Simple Line Interface Calculation) method of Noh and Woodward (1976) and the PLIC (Piecewise Line Interface Calculation) method of van Wachem and Schouten (2002) are two well-known schemes that utilize the line technique. These schemes are based on two steps of reconstructing and propagating the interface. For the SLIC method, simple lines represent the interface where each line is parallel to a certain coordinate axis which depends on the configuration of the interface in the cell. This step is improved to fit the interface through the use of piecewise linear segments in PLIC

method. To propagate the interface, the local velocities are used in each cell and the void fraction is updated afterwards. Another approach that demonstrates efficient interface tracking is based on estimating the interface between two adjacent cells which are called the donor, *D*, and the acceptor, *A*, cells. In this approach, differencing schemes in a form of arithmetic formulas are used to represent the void fraction at the interface, α_f, in terms of the void fraction of the donor, α_D, and acceptor, α_A, cells. This differencing scheme is used to discretize the advection term in Equation 4.2. To avoid the numerical diffusion and ensure compressive character to the interface, high differencing schemes are used. There are several methods that use this approach but the most well-known and efficient ones are the compressive interface capturing scheme for arbitrary meshes (CICSAM) by Ubbink (1997) and inter-gamma compressive by Jasak & Weller (1995).

The interFoam mentioned above which is used by this study adopts the inter-gamma compressive scheme. This scheme is presented by Rusche in his work (Rusche, 2002). Compressing the interface is achieved through another term added to Equation 4.2. As shown below in Equation 4.3, this term appears only in the interface region as $\alpha = 1$ or $\alpha = 0$.

$$\frac{\partial \alpha}{\partial t} + \nabla \cdot (\alpha U) + \nabla \cdot \ [U_r \alpha (1 - \alpha)] = 0 \qquad \text{(EQU 4.3)}$$

Where $U = \alpha U_g + (1 - \alpha) U_l$ and $U_r = U_g - U_l$. These two relationships and Equation 4.2 can be used to derive Equation 4.3. The degree of compression that is caused by U_r at the interface can be adjusted using compression coefficient C_α as

$$U_r(@\text{ the interface}) = \min\left(C_\alpha|U|, \max\left(|U|\right)\right) \cdot \vec{n} \qquad \text{(EQU 4.4)}$$

where n is the unit normal vector of the interface and C_α ranges from 0 to 1. The continuity equation for incompressible flow is $\nabla \cdot U = 0$. The conservation of momentum equation takes into consideration the surface tension effect as shown below.

$$\frac{\partial}{\partial t}(\rho U) + \nabla \cdot (\rho UU) = \\ -\nabla p + \rho f_b + \nabla \cdot \left(\mu(\nabla U + \nabla U^T)\right) + F_s \qquad \text{(EQU 4.5)}$$

For zero gravity environment where the flow becomes surface tension-dominated, the force per volume that affects the gas-liquid interface is represented by Brackbill, et al. (1992) formula of $F_s = \sigma\chi(\nabla\alpha)$ where χ is the curvature of the interface that can be determined using $\chi = -\nabla \cdot \left(\frac{\nabla\alpha}{|\nabla\alpha|}\right)$.

Assuming the two phases are incompressible and with some manipulation, the conservation of momentum equation that govern the fluid dynamics for flow with free surface is

$$\frac{\partial}{\partial t}(\rho U) + \nabla \cdot (\rho UU) = -\nabla p_d + f_b \cdot x(\nabla\rho) \\ +\nabla \cdot (\mu\nabla U) + (\nabla \cdot U) \cdot \nabla\mu - \sigma\nabla \cdot \left(\frac{\nabla\alpha}{|\nabla\alpha|}\right)\nabla\alpha \qquad \text{(EQU 4.6)}$$

Where p_d is the static pressure which takes the form, $p_d = p - \rho(f_b \cdot x)$ and x is the position vector. In most of the cases the body force, f_b is just the gravity, g. The transport equation of α and momentum Equations of 4.3 and 4.6 are the exact equations that are implemented in interFoam solver in OpenFOAM.

It is obvious that the VOF method solves single equation for either the mass conservation or the momentum conservation. The equation deforms to fit certain phase according to the cell region whether it is liquid phase, gas phase, or mixture (the interface region). In this case, the properties and the velocity will be as $\rho = \alpha\rho_g + (1-\alpha)\rho_l$, $\mu = \alpha\mu_g + (1-\alpha)\mu_l$ and $U = \alpha U_g + (1-\alpha)U_l$.

4.2 Geometrical Considerations and Meshing

The geometry of CWRU separator which is introduced in Chapter 1 in Figure 1.1 is shortened as shown in Figure 4.1. This partial geometry in fact is similar to the one used in control-volume approximation.

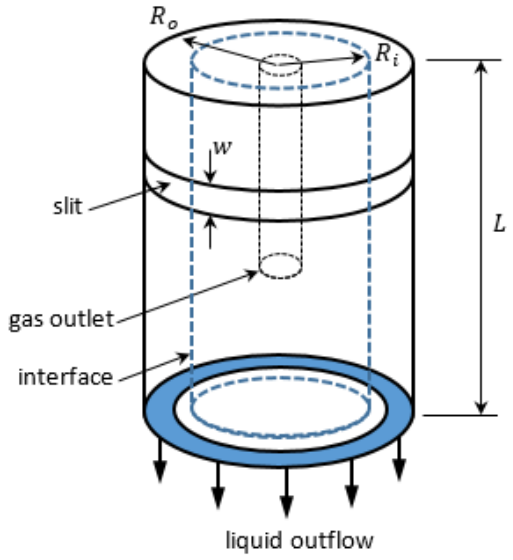

Fig 4.1 Computation domain of the CFD simulation

The figure shows that only the part above the baffle plate is considered thus making the gap between the baffle plate and the separator wall the liquid outlet. The calculation

domain in this case comprises the compartment where the separation process takes place and the configuration of gas core and liquid film is created. Similar to the control-volume approximation, the CFD domain of simulation includes only the section that has two phase flow presence of gas core and liquid annulus configuration. This geometry manipulation is justified due to the fact that the separation process occurs only in that part where most of the transport of mass and angular momentum develop potential variation.

Since the flow domain is treated as an axisymmetric problem (assuming no angular variation to the flow field variables), the computation domain is a wedge at an angle of 5^o as shown in the figure below.

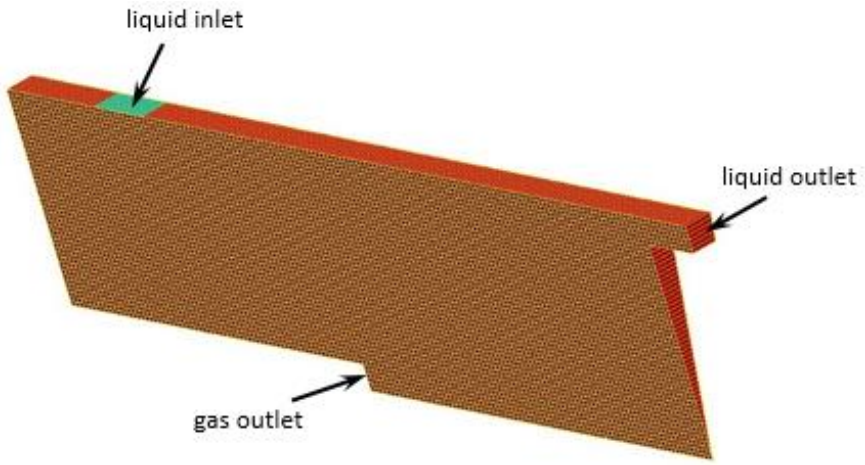

Fig 4.2 Wedge-type meshing of the axisymmetric CFD simulation

Accordingly, a 2-D axisymmetric computational grid is utilized to perform the simulation as shown in Figure 4.3.

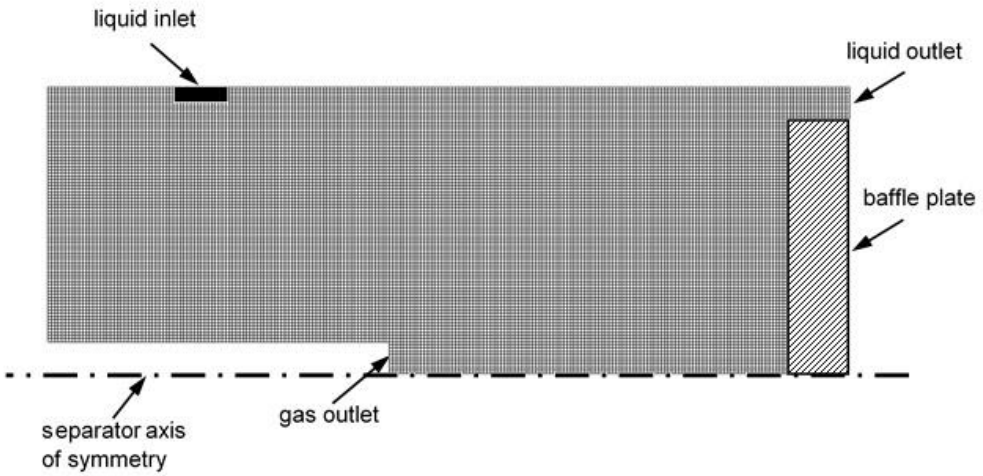

Fig 4.3 Discretization of the computational mesh in the CFD simulation

The grid resolution is kept at grid size of $\delta = (0.112\ \mathrm{mm}^2)^{1/2}$. Grid dependency investigations were carried out to obtain this value as will be discussed later. The number of cells, *N*, in the computational domain can be estimated using (Celik, Ghia, Roache, Freitas, Coleman, & Raad, 2008)

$$\delta = \left[\frac{1}{N}\sum_{i=1}^{N}(\Delta A)_i\right]^{1/2} \qquad \text{(EQU 4.7)}$$

Where $\sum \Delta A$ is the wedge surface area. As an example, the use of the above value of $\delta = (0.112\ \mathrm{mm}^2)^{1/2}$ yields a computational mesh of 90 X 200 (radial X axial) number of cells for wedge area of 28.8 X 82.6 mm (radial X Length). The number of cells changes according to the computational domain size in this study the length of this domain is changed several times to study the effect of aspect ratio, $As = L/R_o$.

The mesh is generated using software utility in OpenFOAM called *blockMesh* and to construct the axisymmetric configuration another utility called *makeAxialMesh* is used.

4.3 Initial and Boundary Conditions

Referring to the control volume analysis of Equation 3.4, it is very fundamental to have sufficient backpressure at the liquid outlet to balance the pressure difference due to the centrifugal force in order to create proper liquid film thickness and hence establishing the separation process. In the experimental separator geometry, the backpressure is created at the liquid outlet which comes after the swirl-stop at the bottom of the separator as shown in Figure 1.1. In the CFD geometry which is similar to the control-volume approximation geometry shown in Figure 4.1, the backpressure is transferred to affect the gap between the baffle plate and the separator wall which constitutes the liquid outlet in this case. At this liquid outlet, the backpressure boundary condition is implemented using the equation

$$\Delta p = \rho K Q^2 \qquad \text{(EQU 4.8)}$$

This equation simulates the valve pressure drop which was previously used in the experiments by Hoyt, et al. (2013) and Kang et al. (2014) . However, for the CFD calculation, the backpressure coefficient, K, is larger as the pressure drop caused by the swirl stopper needs to be taken into account.

Since the CFD simulation in this study utilizes the axisymmetric meshing to discretize the flow domain, the separator inlet is adapted to accommodate the axisymmetric

configuration. The inlet therefore turns into a slit that encircles the separator wall as shown in Figure 4.1. Thus, instead of injecting through a single inlet nozzle at certain location as in the 3-D experimental configuration, the flow is injected through a peripheral slit with width of w. However, this adaptation needs a careful estimate of the amount of mass flow rate and angular momentum that are carried through this slit. This requires that these amounts need to be equivalent to their 3-D values when injecting certain amount of mass flow rate. In other words, this treatment to the injection inlet area to implement the axial symmetry is performed with conserving similar 3-D boundary conditions. By looking at the 3-D injection, the tangential inlet flow through the nozzle delivers both fluxes of angular momentum and mass flow rate. In order to keep similar angular momentum and mass flow rate in the 2-D simulation, the CFD velocity at the inlet is specified as the azimuthal velocity, $U_{\theta,\,2-D}$, and radial velocity, U_r, components which are used to determine the required angular momentum and mass flow rate respectively. The azimuthal component equals the 3-D injection velocity $\left(U_{\theta,\,2-D} = U_{in,\,3-D}\right)$ which is sufficient to ensure a similar angular momentum. This can be achieved through equating the 2-D and 3-D angular momentum as follows

$$\rho R_o Q_{in} U_{\theta,\,2-D} = \rho R_o Q_{in} U_{in,\,3-D} \qquad \text{(EQU 4.9)}$$

The radial component, however, is determined according to the 2-D area used to inject the flow which is a slit of width, w, and thus the injection volumetric flow rate will be $Q_{in} = 2\pi R_o w U_r$. This equation tells us the fact that Q_{in} and U_r are totally independent and the radial velocity component can be any value depending on the slit width. Equalizing this 2-D volumetric flow rate to the one of the 3-D gives

$$wU_r = \frac{D_{in,3\text{-D}}^2 U_{in,3\text{-D}}}{8R_o} \qquad \text{(EQU 4.10)}$$

It is obvious that w and U_r can be any value but for convenience and proximity, the slit width is considered equal to the inlet nozzle diameter of 6.35 mm (0.25 in). Once U_r and $U_{\theta,2\text{-D}}$ are determined, the boundary condition at the inlet can be set up knowing that the inlet pressure is atmospheric gauge pressure and the void fraction is zero (only-liquid injection). The boundary condition at the gas outlet is specified as atmospheric gauge pressure and pure gas (void fraction equals 1) is released. The no-slip condition is applied on all solid surfaces such as the separator walls and the baffle plate surface. The simulation was started by injecting the liquid-only flow through the inlet (the slit) to develop a swirling flow in an empty computational domain (no liquid inventory in the presumably separator compartment). This means that the computational domain of the velocity and pressure fields was initially at zero (assuming gauge pressure). Studying surface tension is always associated with the effect of the contact angle which is identified as the angle between the liquid-gas interface and the solid surface. As it will be seen in Chapter 5, most of the simulations are carried out at contact angle of 90 degrees which is default value in interFoam but it can be changed between 0 to 180 degrees. Since this angle has significant effect on the flow behavior, other results are obtained at different contact angles.

4.4 Grid Dependency

Studying the solution dependency on grid resolution is important in CFD simulations. It is required for the solution in the CFD simulation to be independent from the grid

resolution. This can be achieved by increasing the mesh refinement (increasing the number of grid cells). However, the use of very fine meshes is sometimes computationally expensive and thus it is demanding to do grid dependency analysis to determine the optimum mesh resolution. At this resolution, the results do not change (or only slight changes) with changing the mesh refinement and at the same time not much execution time is required to perform the simulation. To that end, the gird dependency of the mesh configuration mentioned earlier is investigated. CFD simulation is performed to show how certain parameters (the azimuthal velocity in this case) varies as the mesh resolution is changed. Figure 4.4 demonstrates the results of the azimuthal velocity at 0.8 L/min liquid-only injection with aspect ratio and slit width of 1.44 and 7 mm respectively.

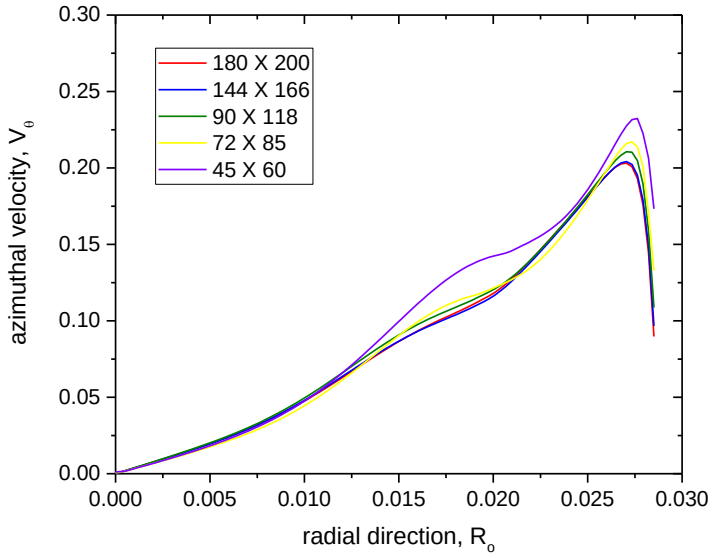

Fig. 4.4 Effect of mesh resolution on the azimuthal velocity as the mesh size changes to several discrete configurations

The results reveal that there is not much change in the azimuthal velocity due to increasing the mesh resolution higher than 90 X 118 number of cells. Accordingly, this intensity of mesh resolution is selected to perform the CFD simulations in this study. The grid size according to Equation 4.7 in this case is $\delta = (0.112\ \mathrm{mm}^2)^{1/2}$ which is the same value mentioned earlier.

Chapter 5 Results

CFD simulation using the VOF technique and control-volume approximation are used to investigate the circumstances that result in a liquid film collapsing inside the CWRU separator mainly for single phase liquid injection. As was discussed in Chapter 3, the flow hydrodynamics depends on several key parameters that are related to the separator geometry, fluid properties and flow field properties. The main concern in studying these parameters is their effects on liquid film thickness, which is significant in indicating how close the flow field is from collapsing. A CFD parametric study is performed to determine which parameters have the most effect on liquid film thickness. The CFD approach is also used to develop a correlation that estimates the skin friction, C_f, which is required for the control-volume approximation. In the CFD approach, axisymmetric meshing is used with some geometrical treatment to implement proper CFD simulation to the flow domain as was discussed in Chapter 4. Most of the simulations in this study were performed at low flow rates due to the fact that in a zero gravity environment, the collapse of liquid film occurs mainly at these ranges where surface tension effects become important.

5.1 Effect of Surface Tension on Swirling Flow

In a microgravity environment, surface tension becomes a critical parameter as the flow rate reaches relatively small values. This can be seen in the CFD results in Figure 5.1 which shows the radial pressure distribution as the surface tension is changed to several values.

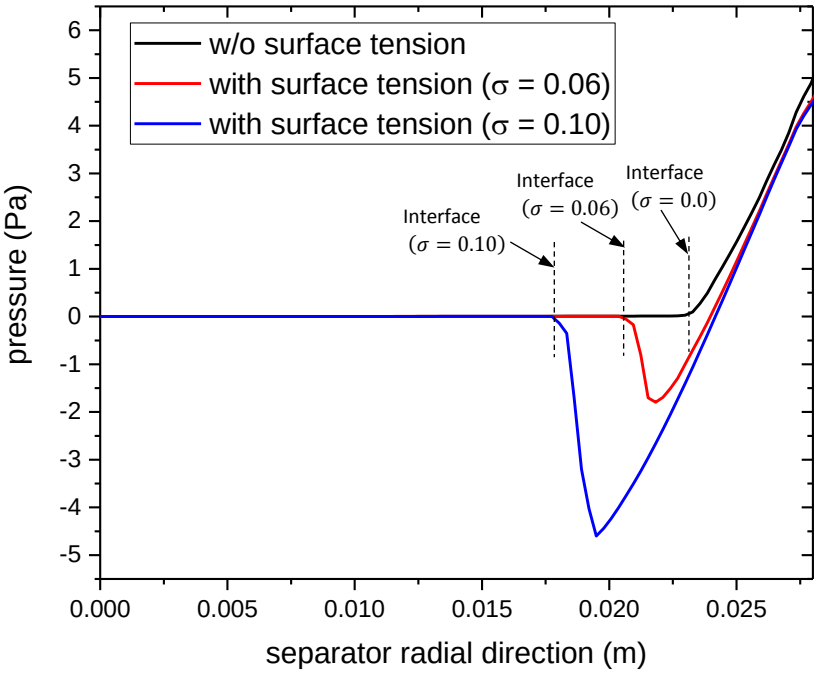

Fig. 5.1 Effect of surface tension on the separator radial pressure as the injection volume flow rate is kept constant at 0.75 L/min

The pressure remains equal to the gas outlet pressure (atmospheric gauge pressure) up to the interface where the surface tension acts. As was discussed in Chapter 3, the pressure at the interface encounters a sudden decrease in accordance with the Young-Laplace equation as

$$p_l - p_g = -\frac{\sigma}{R_i} \qquad \text{(EQU 5.1)}$$

In Fig. 5.1, the injection volume flow rate is constant, which implies a similar azimuthal velocity, so the slope of centrifugally-induced pressure change in the liquid film remains nearly constant. As a result, with increasing surface tension, the film becomes thicker (or

the gas core radius R_i decreases) as seen in Fig. 5.1. The increase of surface tension will lead eventually to the liquid film collapsing as the film becomes too thick.

The effect of surface tension can also be seen with varied injection flow rates as shown in Figure 5.2, which shows how the liquid film thickness changes with the flow rate, with and without surface tension. Both experimental and computational results are presented in the figure.

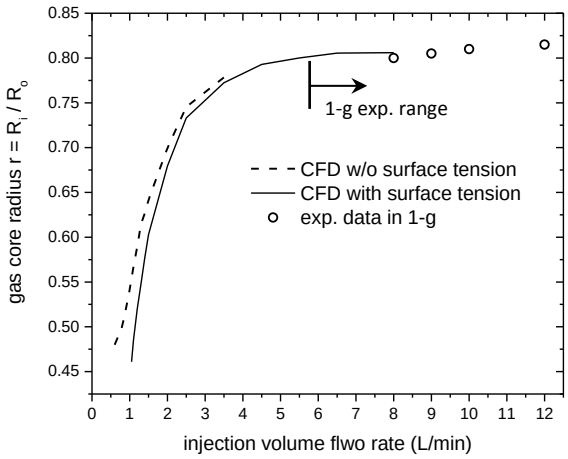

Fig. 5.2 Gas core radius versus broad range of injection volume flow rates with the limits of surface tension effect

The gas core radius is not influenced much by surface tension when the flow rate is above approximately 5 L/min. Below this flow rate, as the flow rate is decreased, the effect of surface tension, which thickens the liquid film as discussed above, becomes increasingly important. However, when the flow rate is above around 1 L/min, the effect of surface tension is not significant. Below about 1 L/min, in Fig. 5.2, the film thickness increases sharply with surface tension, which leads to the film collapsing, which will be discussed

later. As shown in Figure 5.2, the ground-based experimental data are taken at relatively a high injection flow rate (greater than about 6 L/min) to overcome hydrostatic pressure and to establish a proper swirling flow configuration. In this flow rate range, Fig. 5.2 shows that the experimental data agrees well with the CFD results.

As was discussed in the literature review in Chapter 2, the interfacial Weber number is known to be an appropriate quantity to quantify the relative importance of surface tension. Figure 5.3 shows how the Weber number changes with the injection flow rate.

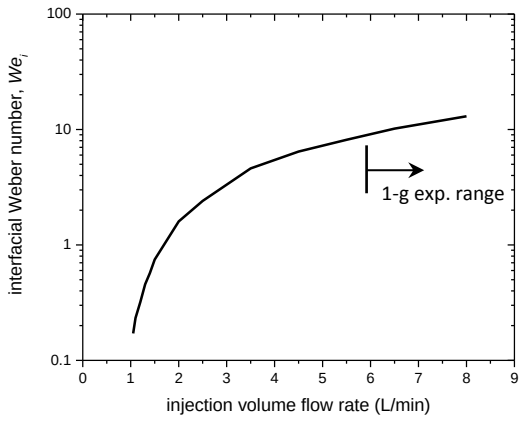

Fig. 5.3 CFD results of the interfacial Weber number against injection volume flow rate for liquid-only injection and zero gravity environment

The figure shows a monotonic increase in Weber number with increasing flow rate as the surface tension effect becomes less important. The increasing trend is expected due to the increase in the azimuthal velocity and gas core radius. As will be shown later, the liquid film collapse occurs when the interfacial Weber number goes below unity. But in

normal gravity tests the smallest We_i is about ten. Therefore, microgravity tests are needed in order to study the liquid film instability.

The previous figures imply that the gas core radius (or liquid film thickness) depends on the injection flow rate. However as discussed in Hoyt, et al. (2013), and will be seen later, any variation in the gas core radius is attributed mainly to the wall friction represented by the skin friction coefficient, C_f. A higher injection flow rate leads to an increase in the injected Reynolds number, which reduces C_f. As a result, the swirling flow gains more angular momentum which yields a thinner liquid film due to the increase in the centrifugal force. Also for low injection volume flow rates, the capillary force plays a large role in determining the gas core radius. In addition to these two parameters of friction and capillary force, however, there are other parameters that need to be investigated. To clarify this point, a parametric study is conducted investigating whether other parameters play any role on sizing the swirl flow inventory (liquid film thickness) inside the CWRU separator.

5.2 Liquid Film Thickness Parametric Study

Since the liquid film configuration can be an indication of the occurrence of instability, it is important to study what parameters dictate the liquid film thickness variation. As was introduced in the control-volume approximation in Chapter 3, the separator hydrodynamics depends on several parameters that are interrelated. Considering all these parameters, the liquid film thickness, h, can be presented as a function of

$\rho, \mu, \sigma, K, R_o, L, A_{inj}, A_{out}$ and U_{in}. Applying dimensional analysis gives dimensionless representation as

$$\frac{h}{R_o} = f(Re_o, We_o, As, \Gamma, \kappa, AR) \qquad \text{(EQU 5.2)}$$

In addition to these quantities, the use of axisymmetric two dimensional simulation in this study introduces one more parameter, the slit width w. Then

$$\frac{h}{R_o} = f\left(Re_o, We_o, As, \Gamma, \kappa, AR, \frac{w}{R_o}\right) \qquad \text{(EQU 5.3)}$$

Studying the effect of any of these quantities on the liquid film thickness requires that the other parameters be kept constant. CFD simulations were performed to study individually each parameter in the equation above. The default values in these simulations are given in Table 5-1.

Re_0	We_o	As	Γ	κ	AR	$\frac{w}{R_o}$
2.1×10^4	114	2.3	82	0.043	17	0.222

Table 5-1 The default case of the parameters that are used in the CFD simulation as only one parameter is changed to study its effect on liquid film thickness

These values are kept constant in all of the simulations except the parameter that needs to be studied.

Using two-dimensional axisymmetric meshing, a liquid-only stream is injected through the slit with a velocity that has azimuthal and radial components for the purpose of acquiring the required angular momentum and flow rate, as mentioned in Chapter 4.

After reaching steady state condition, the liquid film thickness is determined at 10% away from the baffle plate as shown below in Figure 5.4.

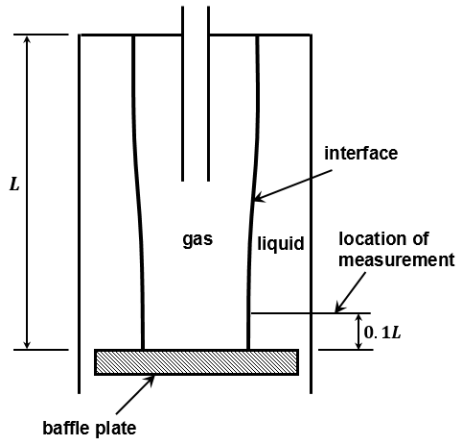

Fig. 5.4 Location of data measurement in CFD simulation

For unstable cases, it is observed that collapsing usually begins close to the baffle plate. Since collapsing is a main concern in this study, this region is chosen to collect data. However, in general, the liquid film thickness can be measured at any location, but not much difference will be observed because for a low injection volume flow rate, the liquid film thickness is mostly uniform in the separator as seen in Figure 5.4.

In addition, since the collected CFD data will be used later in the control-volume approximation, this data therefore should agree with the derivation criteria of the control-volume approximation, namely it considers only the inlet and outlet conditions. Therefore, one needs to collect data close to the liquid outlet. The above 10% location satisfies this condition.

Starting with the slit width, w, as one of the parameters in Equation 5.3 which might have an influence on the liquid film thickness, Figure 5.5 shows that this parameter on average has no effect on the liquid film thickness.

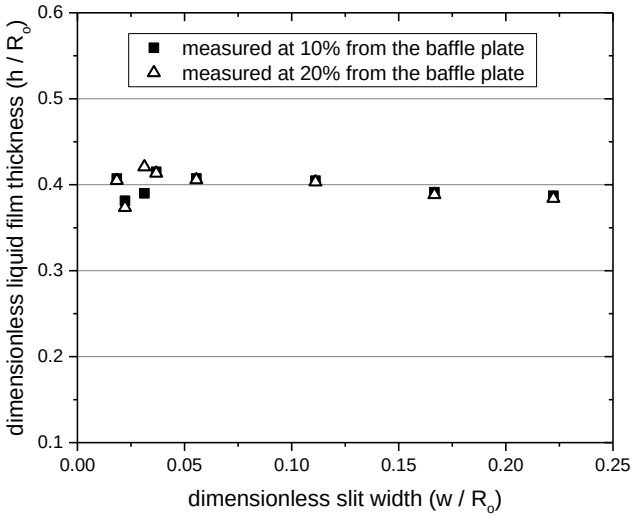

Fig. 5.5 CFD results of the liquid film thickness against the slit width as all other parameters in Equation 5.3 are kept constant

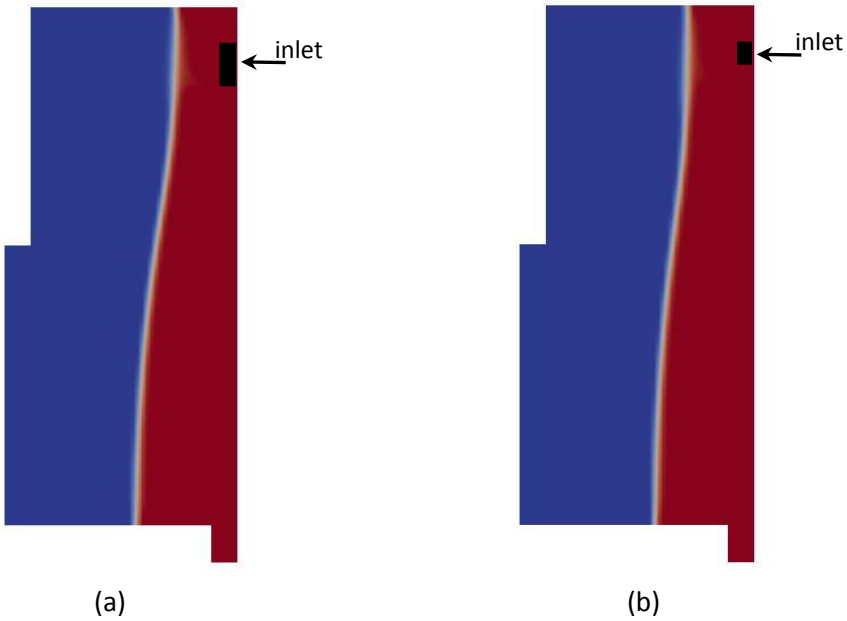

Fig. 5.6 Liquid film contours of CFD simulation for slit width of: (a) 6.4 mm and (b) 0.8 mm

The simulation is carried out using the parameter values presented in Table 5-1 except the slit width. These results are also shown in the liquid film contours of Figure 5.6 at two different slits widths. One conclusion from this simulation is that the slit width can be excluded from any correlation that describes the liquid film configuration. Note that the slit width appears only in the axisymmetric simulation. The fact that the slit width has no influence on the film thickness implies that the injection mode, slit injection or nozzle injection, has no influence. This justifies the present 2-D axisymmetric simulation in place of a more time-consuming 3-D simulation.

The second quantity that is expected to influence the liquid film thickness is the area ratio between the liquid outlet and the nozzle inlet, $AR = A_{out}/A_{inj}$. A_{inj} represents the experimental (or 3-D) injection area and thus for axisymmetric 2-D simulation it is determined using $A_{inj} = Q_{in}/U_{in}$ where U_{in} is equal to the azimuthal velocity component at the inlet.

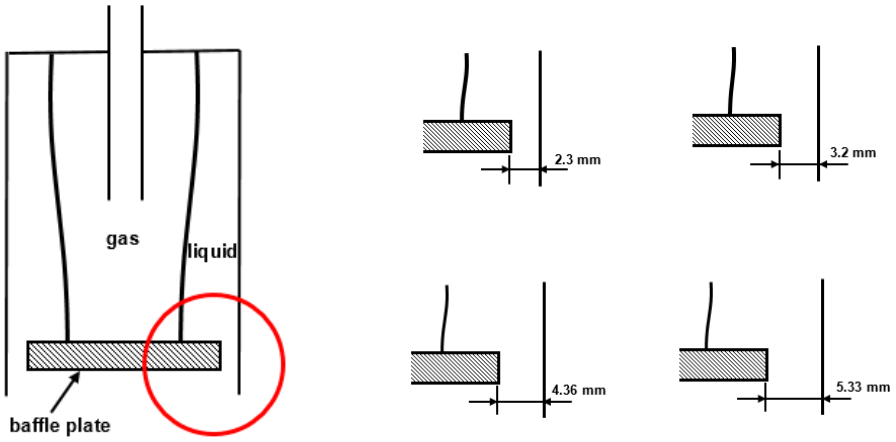

Fig. 5.7 Cases of liquid outlet areas that are used in CFD simulation

This time all other parameters are kept constant which can be achieved by changing only A_{out} as this area has no presence in any of the other parameters described in Equation 5.3. The outlet area, A_{out}, is changed through changing the gap width at four different values as shown in Figure 5.7.

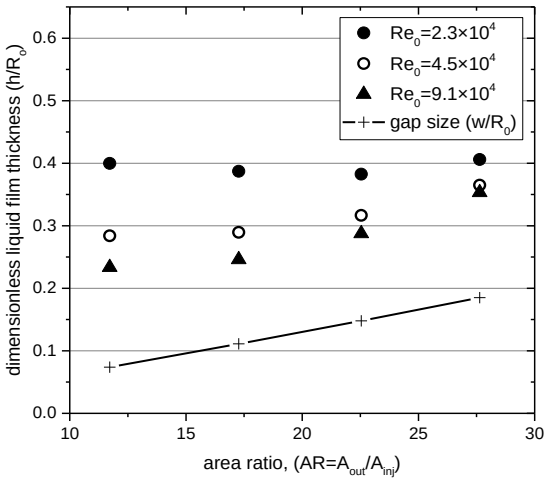

Fig. 5.8 CFD results of the liquid film thickness against the area ratio as all other parameters in Equation 5.3 are kept constant

Since the Reynolds number was found critical in determining liquid film thickness in case of high flow rate injection (Hoyt, et al., 2013; Kang, et al., 2014), the effect of AR is investigated for a range of Re_o.

Fig. 5.8 also shows the size of the gap between the baffle plate and separator inner wall for comparison. The results in Fig. 5.8 shows that the area ratio has an effect on liquid film thickness for a high injection Reynolds number, Re_o, as the film thickness is relatively thin compared to the gap size where the minimum film thickness is about twice that of

the gap size. In comparison, the liquid film thickness is considered to be independent of the area ratio in the range of Reynolds number of present interest.

The third parameter that was computationally investigated is the injected Weber number, We_o. In this study, the Weber number is extremely important as it comprises the effect of capillary force. The results are shown in Figure 5.9 where the liquid film thickness dependency on the injection Weber number is depicted at different injection Reynolds numbers, Re_o.

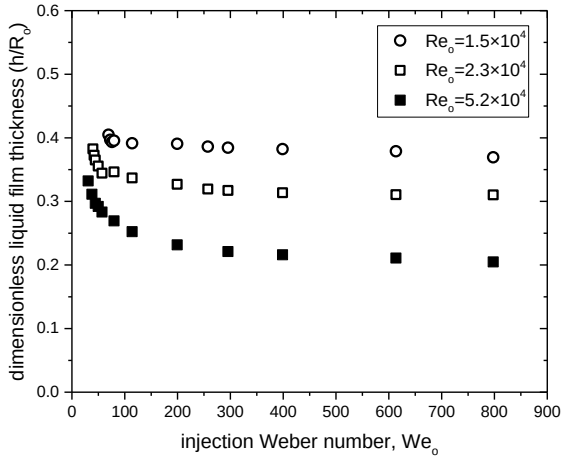

Fig. 5.9 CFD results of the liquid film thickness against We_o at several Re_o as all other parameters in Equation 5.3 are kept constant

The figure shows that the liquid film thickness is not affected by the injection Weber number, We_o, if it is above about 200. Below that value, the liquid film thickness increases as We_o is decreased. Once We_o approaches some lower limits, the influence of capillary force causes a rapid increase in the liquid film thickness. The figure also shows that changing the injection Reynolds number does not affect the general trend of the data

as the change in liquid film thickness demonstrates similar behavior in the three cases of Re_o.

Another parameter to be addressed is related to the separator geometry dimensions which is the aspect ratio, $(As = L/R_o)$. The aspect ratio is a quantity that represents the change of wall friction due to changing the separator length to radius ratio. This means that the increase of separator length leads to diminishing angular velocity as the swirling flow advances towards the liquid outlet as a result of increased wall friction. As was explained earlier, the increase in wall friction yields a thicker liquid film thickness. The quantitative demonstration of such behavior can be seen in Figure 5.10 where the aspect ratio is varied at several values and the other parameters in Equation 5.3 are kept fixed. The effect of As is investigated for three values of We_o in Figure 5.10.

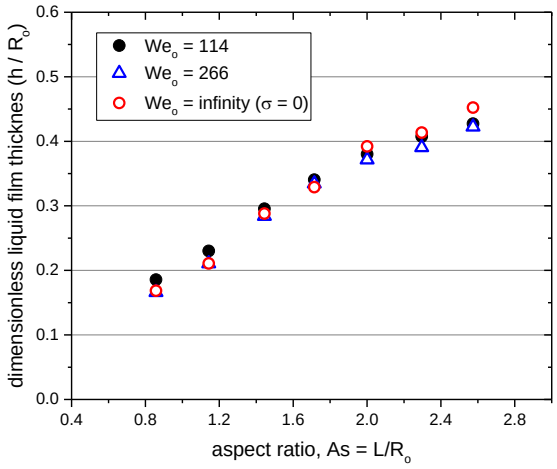

Fig. 5.10 CFD results of the liquid film thickness against the aspect ratio at several We_o as all other parameters in Equation 5.3 are kept constant

It is shown that the liquid film thickness depends mainly on the aspect ratio. For the results shown in Figure 5.10, the injection Weber number has an insignificant influence on the liquid film thickness.

One other dimensionless quantity that is also related to the separator geometry is the area ratio of Γ. As was introduced earlier, this comprises the area ratio between the separator cross section and the injection inlet area with a form of $\Gamma = \pi R_o^2 / A_{inj}$. Referring to the control-volume approximation, this parameter evaluates the change of wall friction with respect to the change of injected angular momentum due to changing the area ratio, $\pi R_o^2 / A_{inj}$. Therefore, it evaluates the similar effect as in the aspect ratio parameter case. But the difference between the two parameters is that for Γ, the effect is caused by an area ratio variation rather than a length ratio variation. CFD simulation is performed to understand how Γ influences the liquid film giving that all other quantities in Equation 5.3 are kept constant at the values described in Table 5-1. The results are presented in Figure 5.11 showing the variation of the dimensionless liquid film thickness against Γ. Similar to the investigation conducted with the aspect ratio, the results are obtained at three different cases of We_o.

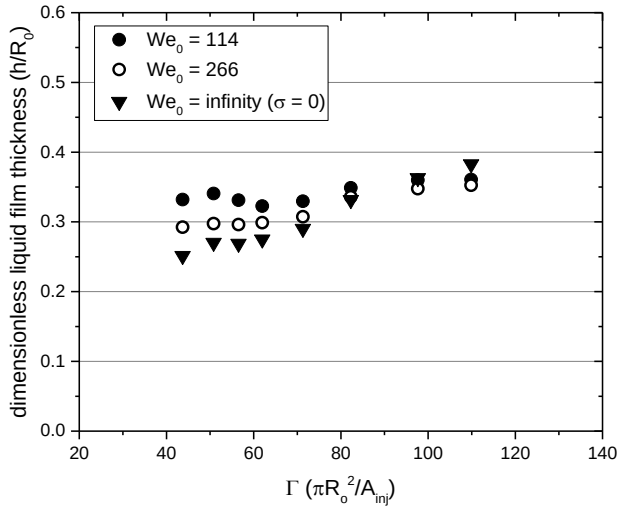

Fig. 5.11 CFD results of the liquid film thickness against Γ at several We_o as all other parameters in Equation 5.3 are kept constant

The figure shows a monotonic increase in the film thickness with increasing Γ when the surface tension effect is negligible (infinite We_o). The figure also shows that the film thickness depends less on Γ with decreasing We_o as the thickness depends more on the Weber number.

One other significant parameter that influences the liquid film is the backpressure at the liquid outlet in the form of the dimensionless backpressure coefficient, κ. This parameter is very important in maintaining a sufficient liquid film thickness as it pushes back against the centrifugal force, hence creating a proper swirling flow configuration for an efficient separation process. Equation 3.17 in the control-volume approximation describes the role of the backpressure by balancing it with the centrifugally-induced pressure surface-tension-induced pressure. From this balancing, it is quite obvious that the backpressure

has an important influence on the separator hydrodynamics. This influence can be seen in the large variation of the liquid film thickness with κ, which was previously found by Hoyt, et al. (2013) for high flow rate injection. A similar conclusion might be observed in this study for low flow rate injection. κ is varied at several values keeping all other parameters fixed. The results are presented in Figure 5.12 where the axisymmetric 2-D CFD simulation mentioned earlier is used to run several cases of dimensionless backpressure coefficients, κ, until reaching a steady state condition such as when the liquid film thickness is computed at 10 % away from the baffle plate. The results are also obtained at different cases of We_o to illustrate the difference between flow domains with varying capillary force intensity.

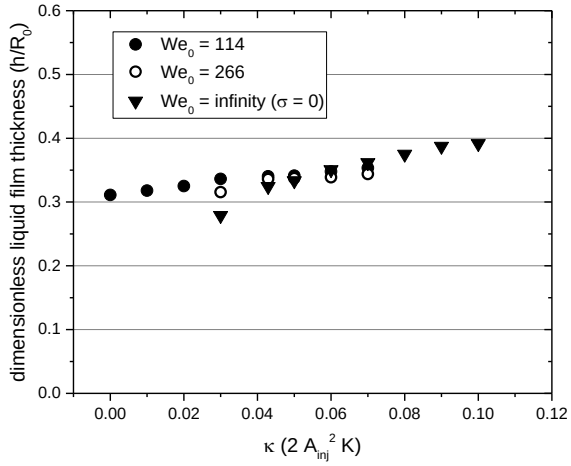

Fig. 5.12 CFD results of the liquid film thickness against κ at several We_o as all other parameters in Equation 5.3 are kept constant

In general, the results depict an increasing trend in all three cases of We_o but each case characterizes a different slope of increase. For low We_o, modest growth behavior is shown. This behavior can be explained using Equation 3.14 which balances the

centrifugally-induced pressure with the surface-tension-induced pressure and the backpressure. In general, any increase in the surface-tension-induced pressure and the backpressure is balanced by the centrifugally-induced pressure by increasing the liquid film thickness. It is obvious that the surface tension term $(2/We_o r_i)$ becomes significantly important at low We_o. For instance, with the case of $We_o = 114$ $(r_i = 0.66)$, surface tension contributes an effect against the centrifugally-induced pressure $(u^2(1 - r_i^2))$ of more than 46% of the total effect, The other 54% comes from the backpressure term represented by κ $(\kappa = 0.03 \text{ in this case})$. Thus in this case of low We_o, the liquid film thickness needs to be thicker to increase the centrifugally-induced pressure in order to balance the surface-tension-induced pressure and the backpressure. At a high We_o, the surface-tension-induced pressure diminishes and only the backpressure remains, therefore the centrifugally-induced pressure requires a thinner liquid film to encounter and balance only the backpressure effect. It is noticeable that the liquid film thickness at low We_o, is constant even with the increase of κ. This is in fact attributed to the increase in azimuthal velocity as κ increases, which causes an increase in the centrifugal-induced pressure and therefore there is no need to increase the liquid film thickness to balance the increase in the backpressure.

Another parameter that is expected to affect the liquid film thickness through wall friction is the injection Reynolds number Re_o. Figure 5.13 shows its effect on the film thickness.

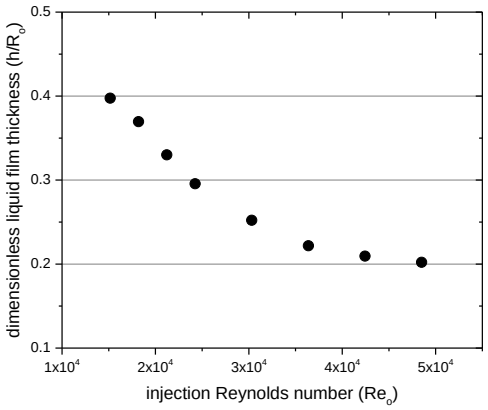

Fig. 5.13 CFD results of the liquid film thickness against Re_o as all other parameters in Equation 5.3 are kept constant

The results show the liquid film thickness decreases with increasing Reynolds number. With increasing Reynolds number, C_f decreases as inertia effects become more important compared to the viscous effects, which results in a thinner liquid film as discussed earlier.

5.3 Skin Friction Coefficient for Control-Volume Approximation

This section is intended for developing a skin friction coefficient correlation using the CFD data results. Since the skin friction coefficient is needed in the control-volume approximation, a correlation for this coefficient needs to be developed.

The procedure to determine the skin friction coefficient from the CFD results of the liquid film thickness is as follows. Using Equation 3.17 and with the CFD result of the gas core radius r_i, the dimensionless tangential velocity of u, can be determined as

$$u = \left[\frac{2}{We_o(r_i - r_i^3)} + \frac{\kappa}{(1 - r_i^2)}\right]^{1/2} \quad \text{(EQU 5.4)}$$

Once u is determined, the skin friction coefficient can be obtained using

$$C_f = \frac{1 - u}{\Gamma A s u^2} \quad \text{(EQU 5.5)}$$

Similar to the earlier dimensional analysis, it can be shown that

$$C_f = F(Re_{0,}\, We_0, As, \kappa, AR) \quad \text{(EQU 5.6)}$$

Based on our earlier analysis (Kharraz, et al., 2016), it is appropriate to correlate C_f in terms of the liquid film Reynolds number, Re_f, which was already introduced in Chapter 3 as

$$Re_f = \frac{\rho U_\theta (R_o - R_i)}{\mu} = Re_o u(1 - r_i) \quad \text{(EQU 5.7)}$$

It is found that C_f depends mainly on Re_f in the parametric range of interest. The effects of other parameters are felt implicitly through u and r_i. Similar to the high flow rate case that was studied by Hoyt, et al. (2013), the skin friction coefficient correlation in this study is also found in the form of $C_f = C\left(Re_f\right)^{-n}$. Figure 5.14 shows the result of C_f against Re_f. The high flow rate injection case of Hoyt, et al. (2013) is also shown for comparison. The data regression of this figure gives a correlation as

$$C_f = 51 {Re_f}^{-0.92} \quad \text{(EQU 5.8)}$$

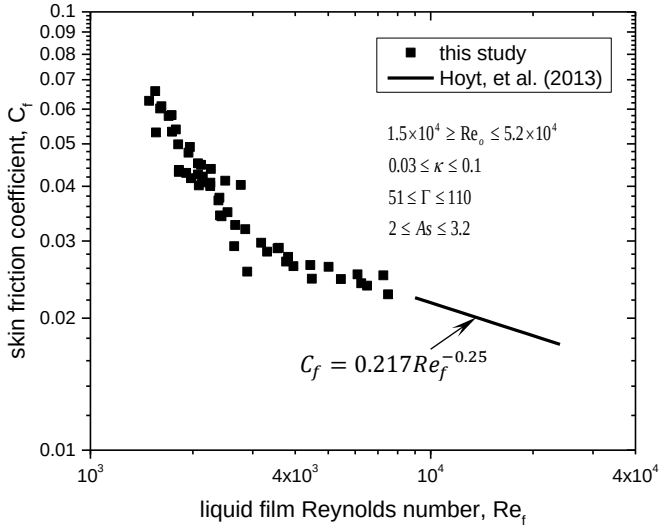

Fig. 5.14 Skin friction coefficient as a function of Re_f using data from CFD simulations at several ranges of Re_o, κ, As, and Γ

The figure shows that the skin friction coefficient depends more strongly on Re_f in the present parametric range than in the higher Re_f range of Hoyt, et al. (2013). The fact that the slope of Re_f is nearly equal to -1 indicates that the flow is nearly laminar.

To validate the obtained C_f correlation, the gas core radius $(r_i = R_i/R_o)$ is obtained using Equations 3.16 and 3.17 in the control-volume approximation and compared with the CFD results. For several cases of κ, Γ, and As, the above expression is used to determine C_f and hence the liquid film thickness can be calculated using the above mentioned equations. The results are shown in Figure 5.15. The comparison shows reasonable agreement near the bottom of the separator between the two approaches.

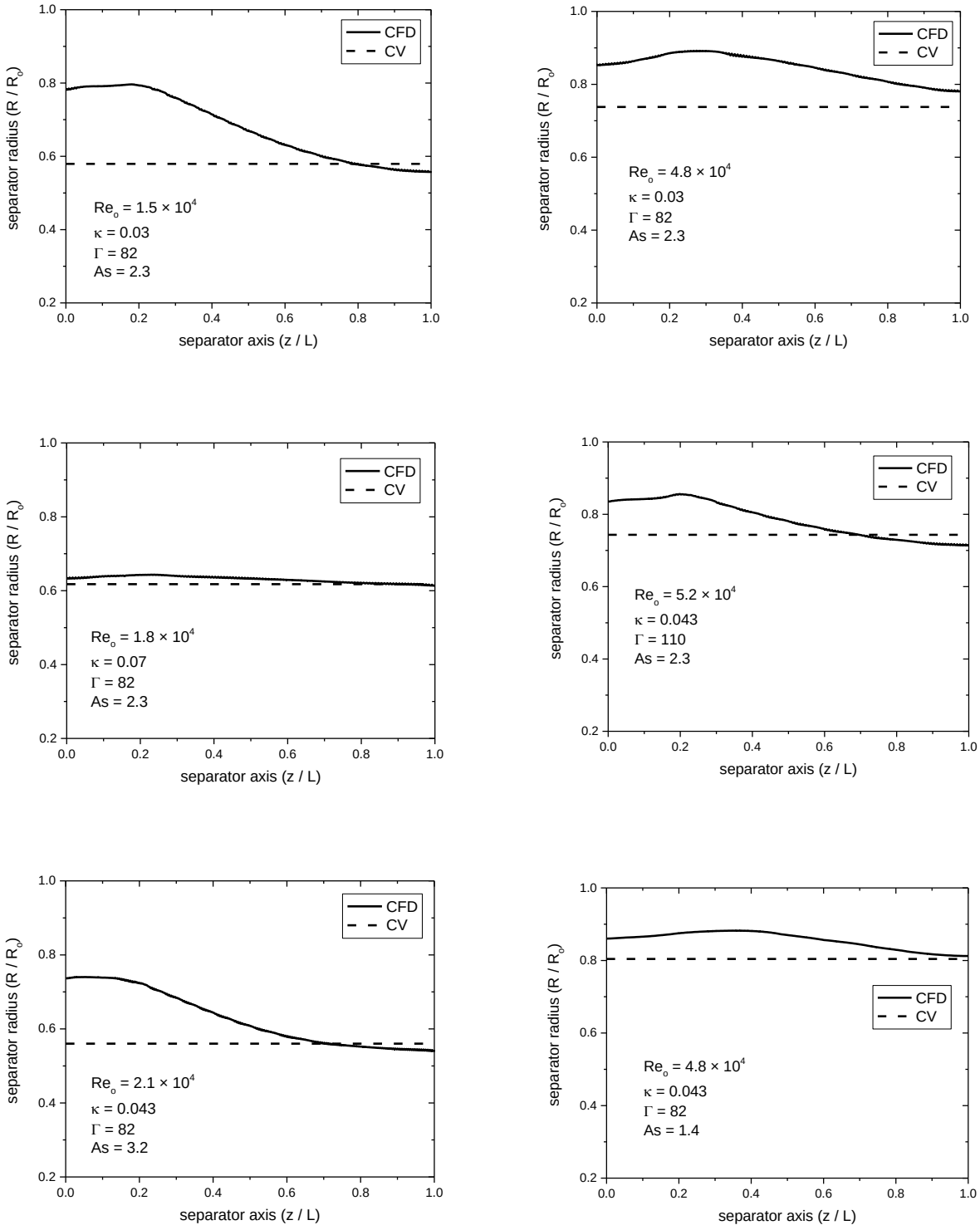

Fig. 5.15 Liquid film thickness comparison between CFD and control-volume approximation for several cases of Re_o, κ, As, and Γ

The skin friction coefficient correlation of Equation 5.8 is one required step to study the stability of liquid film using the control-volume approximation approach. In this approach, once C_f is known, the liquid film thickness and the maximum azimuthal velocity can be determined. Therefore, with these two parameters known,, the interfacial Weber number can be obtained at any injection flow rate. The upcoming section presents the significance of this parameter.

5.4 Stability of Swirling Flow

This section starts addressing the main objective of this study which is the liquid film stability. Both approaches of control-volume approximation and CFD are utilized in the investigation. Since the problem of this study characterizes continuous incoming flow, the flow field behavior changes in the axial and the radial directions. This change appears in a form of reduction in the azimuthal momentum in the axial direction which produces thicker liquid film close to the liquid outlet (at the bottom of the separator). The decrease in the azimuthal momentum which implies decrease in the centrifugal force is associated with an increase in the capillary force. To estimate the scale of influence of each force, the dimensionless quantity of Weber number is employed which is the commonly used quantity in this case (Bean, Waghela, Kurwitz, & Best, 2002; Klein, 2009; Supak, 2007). As Weber number goes to lower values, the liquid film becomes closer to experience collapsing in critical cases. The minimum Weber number value that is close to collapsing is referred in this work as the critical value that limits the event of liquid film collapsing. Figure 5.16 is a CFD data collected at several injection Weber number.

As the figure shows, reducing the injection Weber number, We_o, which implies decrease in the centrifugal force leads to decrease in the interfacial Weber number, We_i. This parameter minimizes in the direction toward the bottom of the separator where it eventually reaches the lowest value.

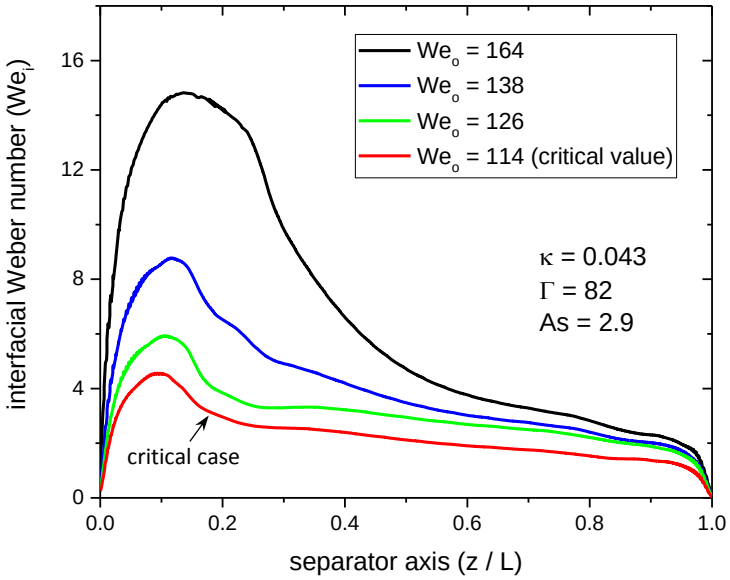

Fig. 5.16 CFD results of interfacial Weber number along the separator axis at several injection Weber number cases as κ, As, and Γ are kept constant

The separator bottom region therefore is very important in this study as the centrifugal force at its weakest level and hence any liquid film collapse is expected to happen in this region. For this reason, the CFD data is collected from that region at 10% away from the baffle plate as mentioned earlier and Weber number of the critical case at this location is considered as a limit before collapsing. Experiencing liquid film collapsing in the current problem is caused by the unbalance forces at the interface which can be evaluated using Weber number. In addition, the swirling flow characterizes moving interface in which the

interface location is part of the solution. Those aspects really differentiate the present work from the stability of rotating liquid films with fixed interface which in this case the theory of hydrodynamic stability is usually used. One simple case with fixed interface is investigated in the next section.

5.4.1 Stability of Solid Body Rotation

This section addresses the case when no inflow and outflow is part of the problem. As a results the interface is radially-fixed which is not the case in this work. Any instability to such interface occurs as a results of amplifying disturbance and the problem is a linear hydrodynamic stability problem in this case as mentioned earlier in Chapter 2. Using this approach, Samsonov (1971) studied solid body rotation of an arrangement of gas core and an infinite liquid film thickness as shown in Figure 5.17. It is noticeable in his figure that the side walls are curved. This is for the purpose of obtaining less than 90^{o} contact angle at the interface ends. The intention here is to convey that those ends are fixed as with small contact angle the liquid faces more resistance to slip.

He reached stability criteria in terms of the interfacial Weber number $(\rho\omega^2 R_i^3/\sigma)$ and the gas core aspect ratio of (H/R_i) as expressed in Equation 5.8.

$$We_i \geqslant \frac{1}{2}\left[1 - \frac{4\pi R_i^2}{H^2}\right] \qquad \text{(EQU 5.9)}$$

The correlation shows that the decrease of aspect ratio (R_i/H) brings more instability to the gas core as higher Weber values are required to establish stable gas core.

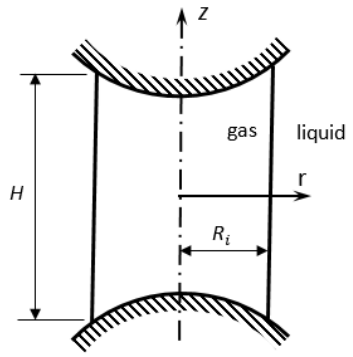

Fig. 5.17 Gas-liquid configuration used by Samsonov

To show that the stability of solid body rotation is different from the present work stability, CFD simulation results is obtained for this type of flow. A configuration of gas core and liquid film is rotated as solid body rotation with angular velocity ω. Axisymmetric two-dimensional meshing is used in the computation. Several cases are simulated with different liquid film thicknesses and aspect ratios. Stable and unstable results are obtained depending on Weber number and aspect ratio as described by Samsonov. For unstable cases at relatively low Weber number and high aspect ratio, the collapsing is achieved in a form of two different modes as shown in Figure 5.18a and 5.18b.

The collapsing in the first mode is encountered at the interface ends while the collapsing in the second mode occurred at the middle. Encountering the first mode which is physically easier to occur is due to having lower interfacial Weber number compared to the case with the second mode. In addition, the collapsing in the second mode is achieved through making low pressure location near the interface which creates pressure gradient with the surrounding region and as a result mass flow moves toward that location and causes collapsing.

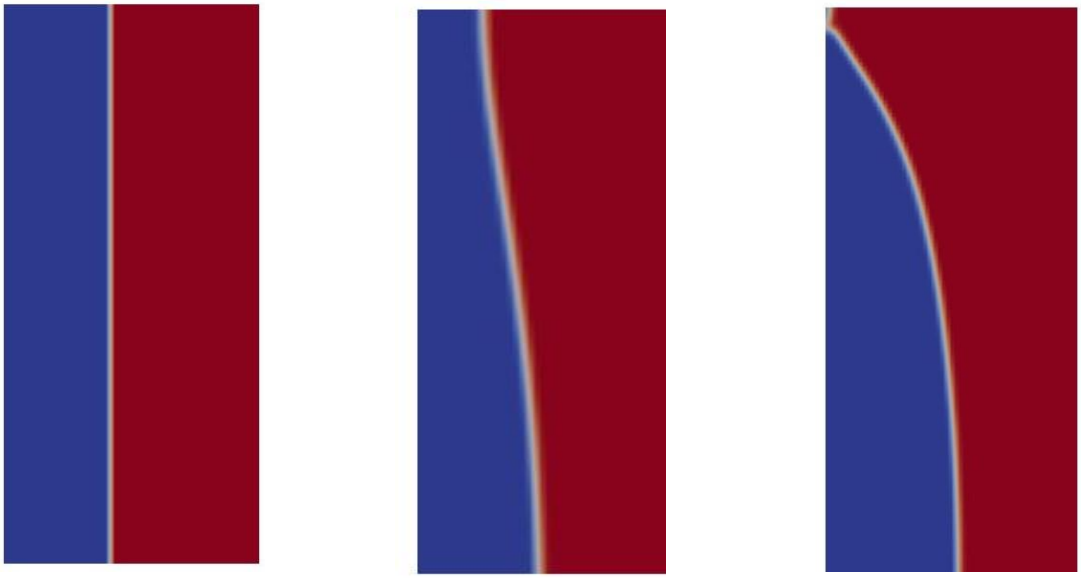

(a) First mode of collapsing

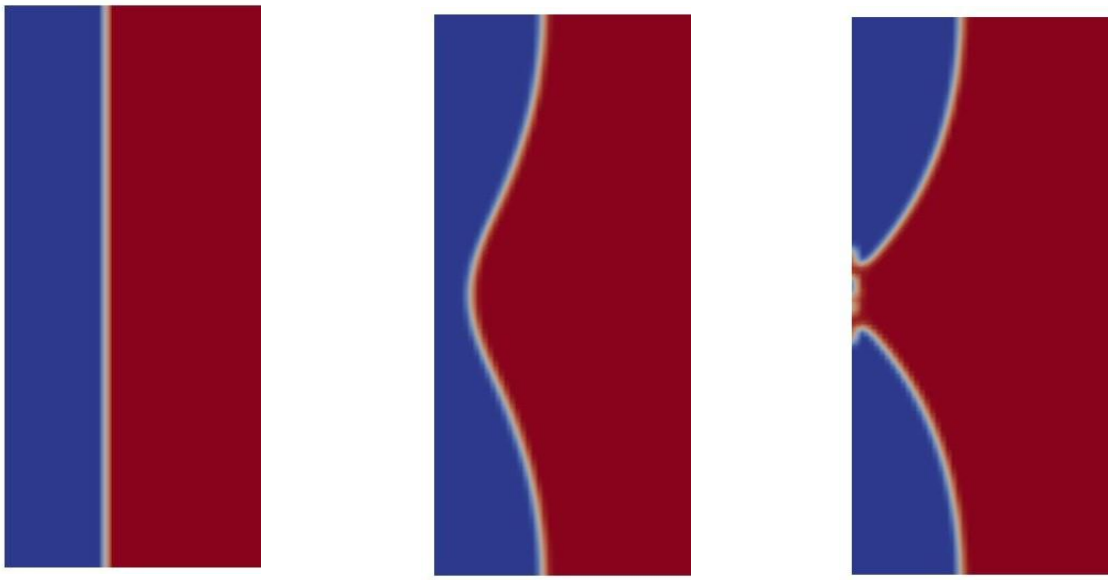

(b) Second mode of collapsing

Fig. 5.18 Liquid film collapsing for solid body rotation using CFD simulation for: (a) $H/R_i = 6$ and $We_i = 0.23$ ($\omega = 4$ rad/s) and (b) $H/R_i = 6$ and $We_i = 0.36$ ($\omega = 5$ rad/s)

All of the CFD results of the stable and unstable cases are shown in Figure 5.19. Samsonov criteria results are also included in order to get sense and make comparison with the CFD results.

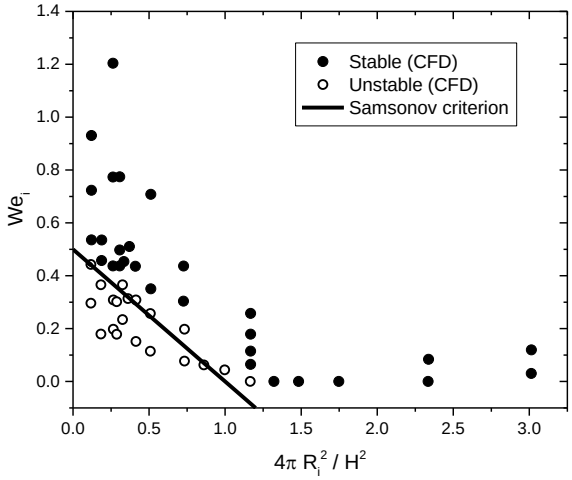

Fig. 5.19 CFD simulations and Samsonov correlation for flow field of gas core and liquid film rotating as solid body rotation

The CFD results agrees well with Samsonov criteria. It is noticeable that some stable case are achieved at no rotation $(\omega = 0)$ which can be also obtained using Samsonov criteria in Equation 5.9.

As mentioned earlier, the solid body rotation approach does not consider other parameters effect such as the friction at the wall. Also there is no injected flow and therefore no moving boundaries which differentiates solid body rotation from the current problem of this study. Since this study is mainly concerns swirling flow inside cyclonic

separators, the injected flow, the interface, and wall friction play a big role in the liquid film stability as it will be seen later.

5.4.2 Stability of Liquid Film in CWRU Passive Cyclonic Separator

This section clarifies in details that the stability of liquid film in separators is different from the one explained in the previous section. Moving interface in this case leads to variation in centrifugal and capillary forces knowing that the balance between them plays a big role in the stability of liquid film. Other parameters such as the skin friction coefficient is also important. As it will be shown later, the increase of skin friction coefficient which implies an increase in the friction force at the wall is expected to require higher interfacial Weber number to establish stable liquid film. This is in fact due to the decay in the centrifugal force as the azimuthal velocity decreases. This gives the understanding that instable liquid film can be reached through decreasing the interfacial Weber number. One way to achieve that is by decreasing the injection Weber number until experiencing liquid film breakdown. This approach is initially applied in this study in case of constant skin friction coefficient which gives primary estimation to critical Weber number. The results in this case are obtained using the equations developed in control-volume approximation where analytical and numerical solutions are reached. The analysis revealed a remarkable observation of an interfacial Weber number exactly equals one regardless of the values of the other parameters. The control-volume approximation equations are previously introduced in Chapter 3 and by taking Equation 3.16 we can write

$$\Gamma A s u^2 C_f + u - 1 = 0 \qquad \text{(EQU 5.10)}$$

It is quite obvious that for certain separator geometry, u is always constant as long as C_f is constant. In addition, Equation 3.17 with some arrangement gives

$$F(r_i) = r_i^3 + \left(\frac{\kappa}{u^2} - 1\right) r_i = \frac{-2}{We_o u^2} \qquad \text{(EQU 5.11)}$$

Decreasing the injection Weber number, We_o, as u and κ are kept constant, will decrease the equivalent, $F(r_i)$ and the dimensionless gas core will be also reduced. Continuing to go to lower We_o brings Weber number to the critical value where the gas core radius is minimum. Analytically this minimum can be achieved by setting the derivative of $F(r_i)$ equals to zero. Therefore,

$$\frac{dF(r_i)}{dr} = 3r_i^2 + \frac{\kappa}{u^2} - 1 = 0 \qquad \text{(EQU 5.12)}$$

Thus,

$$r_{i,\,\min} = \left(\frac{1}{3}\right)^{(1/2)} \left(1 - \frac{\kappa}{u^2}\right)^{(1/2)} \qquad \text{(EQU 5.13)}$$

At this value of gas core radius, the injected Weber number is at the lowest possible value to establish stable liquid film. By substituting the expression of $r_{i,\,\min}$ into Equation 5.11, the critical value of injected Weber number will be,

$$We_{o,\,\min} = \frac{3}{\left(\frac{1}{3}\right)^{(1/2)} \left(1 - \frac{\kappa}{u^2}\right)^{(3/2)} u^2} \qquad \text{(EQU 5.14)}$$

According to this equation and to ensure stable liquid film the injected Weber number must be equal or greater than this critical value. The critical interfacial Weber number can be determined using $We_i = r_i^3 u^2 We_o$ which is mentioned earlier in Chapter 3. Using the expressions specified for $r_{i,\,\min}$ and $We_{o,\,\min}$ in the equations above, the critical Weber number at the interface will end up to $We_{i,\,\min} = 1$.

Similar result is achieved through numerically solving Equations 3.16 and 3.17 in the control-volume approximation considering the skin friction coefficient constant as show in Figure 5.20.

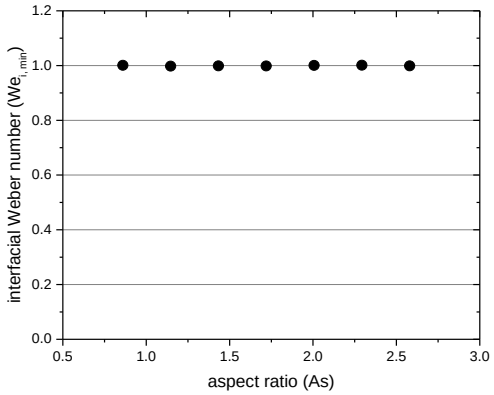

Fig. 5.20 Control-volume approximation results for interfacial Weber number against aspect ratio as C_f is kept constant

This figure shows critical interfacial Weber number of unity as the aspect ratio is changed. Similar results can also be obtained for the other parameters of κ and Γ.

This outcome tells that having the skin friction coefficient constant disables the effect of any other parameter. Therefore, and based on the control-volume approximation approach, the skin friction coefficient is the key parameter in dictating instability of liquid film in passive cyclonic separators. However, since realistically this coefficient depends on We_o, Re_o, κ, Γ, and As, all these parameters needs to be investigated in order to understand the whole picture on which parameter that is significantly affects the stability of liquid film.

To achieve this task, control volume analysis and CFD approaches are utilized. In the first approach, Equations 3.16 and 3.17 are solved simultaneously to find r_i, u at certain We_o and thus the interfacial Weber number, We_i. Equation 5.8 is used to represent the skin friction coefficient in the calculation. Solving these two equations is repeated with decreasing injection Weber number, We_o, until achieving the lowest possible value (the minimum) of We_i where after this value no solution can be obtained. The accuracy of collapsing condition was up to four decimal places of We_o. The results of such investigation is intended to give more details of which parameter affects the stability of liquid film the most. Figure 5.21 shows control volume analysis results based on the injected flow condition.

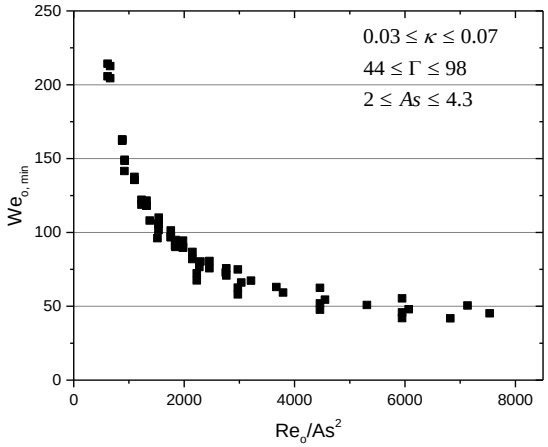

Fig. 5.21 Control-volume approximation results for critical injection Weber number at specific ranges of κ, Γ, and As with varied C_f

The use of injection Weber number and Reynolds number to dictate the liquid film collapsing gives an advantage to predict this event from known parameters. In this figure,

the values of $We_{\mathrm{o,min}}$ are plotted against $Re_o/As^{2.0}$, which shows a good correlation of all the data in the present parametric range. It is quite obvious that the increase in Re_o brings more stability to the liquid film thickness as less $We_{o,\,\mathrm{min}}$ is required to avoid collapsing. This is attributed to the decrease in C_f which leads to less angular momentum loss due to friction. Also, the liquid film is sable as long as the ratio of Re_o/As^2 is constant as the other parameters such as κ and Γ have insignificant effect in this case. The figure shows that the aspect ratio is in quadratic relation with the critical Weber number. This is consistent with the assumption of solid-body rotation behavior of control-volume approximation as this quadratic form is also achieved by Samsonov who assumes similar behavior. Also as was early introduced in Chapter 3, the radius of curvature (equals the gas core radius in this case) which determines the surface tension effect has quadratic relation with the aspect ratio.

The effect of C_f parameter represented by We_o, Re_o, κ, Γ, and As on the stability is also investigated using the CFD approach as a second approach intended to be also used in this work. Similar to the control-volume approximation, several cases of these parameters were simulated. The collapse condition is achieved through an incremental increase in the surface tension as the other parameters are maintained constant. Due to the computation time restriction during CFD simulations, the surface tension increment cannot be too small to a degree where the computation time becomes very costly. Moreover, it is not possible to find the collapse condition accurately because near the critical point and due to small numerical disturbances, the core may collapse if we run the

case for several days. For this reason the incremental change used in the present simulation is 5 % of the Weber number. Once the collapsed condition is achieved, the preceding condition is the one that is sought as its results of interfacial Weber number is close to collapsing. The CFD results are shown in Figure 5.22 with the control-volume approximation results which is the regression curve of the results in Figure 5.20.

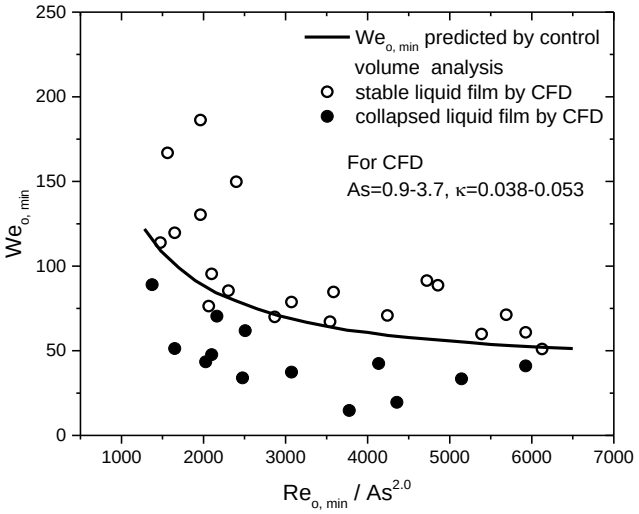

Fig. 5.22 Minimum (critical) injection Weber number of CFD and control-volume approximation results at specific ranges of κ, Γ, and As with varied C_f

The CFD results show both stable conditions just before collapsing and the conditions for the collapsed liquid film. It is noticed that when Re_o is relatively small, the collapsing process is very slow so that the error involved in finding the collapse condition increases. Moreover, according to Figure 5.23, the critical Weber number increases sharply when the parameter $Re_o/As^{2.0}$ is small, which makes it difficult to identify the collapse condition accurately in the CFD. For those reasons, the range below $Re_o/As^{2.0}$ of 1000 is not included in the comparison. Overall, the agreement between the control-volume

approximation and the CFD simulation is reasonable. Knowing that the control-volume approximation can be performed much faster than the CFD simulation, the former approach can be used as a tool in selecting the operational range for a microgravity experiment. The figure reveals that the liquid film is more stable at higher Re_o and lesser As. This trend in the minimum Weber number is attributed to the high centrifugal force at the interface.

Figures 5.21 and 5.22 describe the liquid film stability using the inlet condition. However, it is also important to investigate what is the condition at the interface which is in fact the place where is collapsing takes place. Figure 5.23 shows critical interfacial Weber number, $We_{i,\,\min}$, against liquid film Reynolds number, $Re_f\ (= u(1-r_i)Re_o)$. $We_{i,\,\min}$ is used by several authors (Bean, Waghela, Kurwitz, & Best, 2002; Klein, 2009; Supak, 2007) to identify liquid film collapsing. For this study, Re_f is an adequate parameter to describe the flow characteristics of the liquid film.

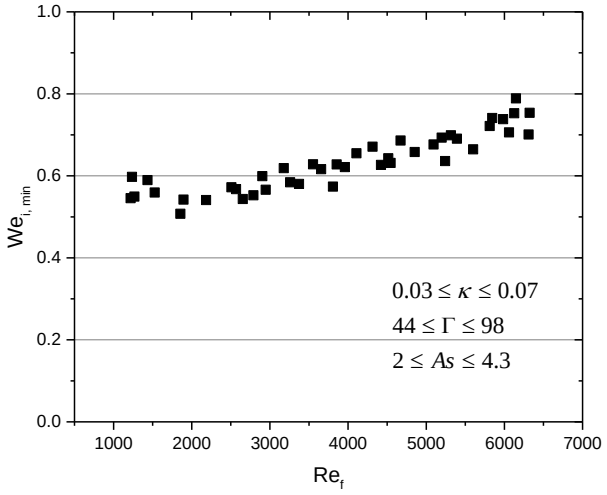

Fig. 5.23 Minimum (critical) interfacial Weber number results obtained using control-volume approximation at specific ranges of κ, Γ, and As with C_f

It is noticeable that As, κ, and Γ have slight effect on the minimum interfacial Weber number, $We_{i,\min}$. In addition, Figure 5.22 reveals that $We_{i,\min}$ is an explicit function of Re_f. The increasing trend of $We_{i,\min}$ is due to the decrease in skin friction coefficient as Re_f increases. That leads to an increase in gas core radius, r_i, as well as the azimuthal velocity, u, giving that $We_i = We_o r_i^3 u^2$. In the meantime however, the minimum injection Weber number,$We_{o,\min}$ results exhibits decreasing trend as was shown earlier. Figure 5.23 also shows that the gas core collapses when $We_{i,\min}$ is about unity. This number is much smaller than the values obtained in the aforementioned parabolic flight tests by Bean, et al. (2002), but it is close to the value obtained in the analysis by Samsonov (1971) for the pure solid-body rotation case without injection. Physically, unit-order Weber number means that the surface tension is on the same order as the centrifugal force, which makes sense because the core collapses only when the surface tension becomes important.

The use of the injection Weber number to demonstrate the critical stability condition is also performed using CFD approach and the results are plotted along with the control-volume approximation results as shown in Figure 5.24. This figure can also be considered as a comparison between control-volume approximation prediction and CFD results. The CFD interfacial Weber numbers are obtained at interface location where collapsing commonly initiates. This location is found mostly at 90 percent of the separator

computation length starting from the top as shown previously in Figure 5.4. Beyond this location, the wall friction starts to affect the tangential velocity.

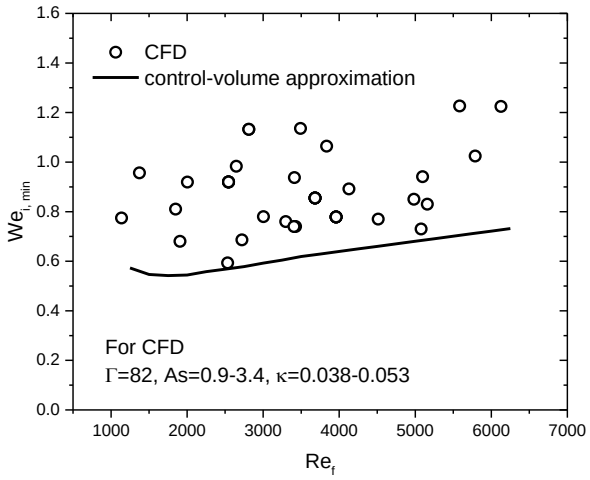

Fig. 5.24 Minimum (critical) interfacial Weber results obtained using CFD and control-volume approximation at specific ranges of κ, Γ, and As with varied C_f

The CFD results are higher than the control volume analysis which is reasonable. This is due to the control-volume approximation assumption of solid body rotation as no axial variation is considered in this approach. This implies that no decay to the angular momentum in the axial direction starting from the injection port takes place. As a result the control-volume approximation is more stable than the CFD simulation where in this case the azimuthal velocity declines due to the side wall friction as the flow advances toward the liquid outlet in the axial direction. Consequently, the swirl flow loses some of its angular momentum which means becoming more susceptible to collapsing. One evidence on this behavior is the increase in liquid film thickness in the same direction of

decaying angular momentum as shown in Figure 5.25a. In addition the collapse consistently starts at the bottom of the separator and close to the baffle plate as shown in Figure 5.25b where the angular momentum reaches minimum while the surface tension force at its maximum value.

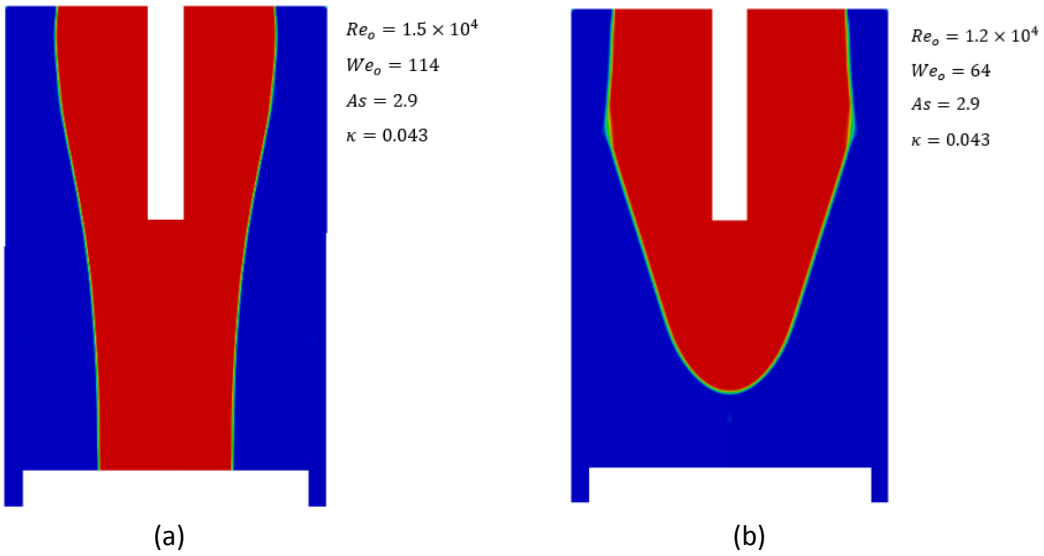

Fig. 5.25 CFD results contour for two different cases of: (a) stable case with variation in liquid film thickness in the axial direction and (b) collapsed case

All Weber number results affirm that Reynold number dominates over all of the other parameters in creating changes. This implies the fact that most of the influence of the coefficient of friction, C_f, on the liquid film stability is attributed to Reynolds number. Referring to Figure 5.23, it is quite evident that the effect of κ is insignificant on the stability. Also not much influence the aspect ratio demonstrates on the results which can be also shown in Figure 5.26 below.

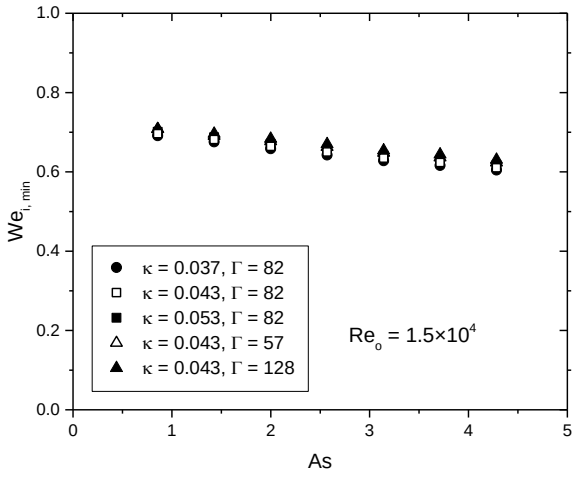

Fig. 5.26 Minimum (critical) interfacial Weber number against aspect ratio obtained using control-volume approximation at several sets of κ and Γ and constant Re_o

Control-volume approximation is used to obtain this figure. As was explained earlier, Equations 3.16 and 3.17, are solved simultaneously to find the lowest interfacial Weber number, $We_{i,\,\min}$, at several aspect ratios, As, as the parameters of κ and Γ are kept constant at certain values and this procedure is repeated for many different values of these parameters as shown in the figure. The solution shows that $We_{i,\,\min}$ is independent from κ and Γ but demonstrates slight dependency on the aspect ratio.

5.5 Effect of Contact Angle on Stability of Liquid Film

All of the previous CFD results are obtained at 90^o contact angle. In reality however, the contact angle is different sometimes and that raises the question what consequence has

this angle on the results if it is changed to different value. Therefore, further CFD simulation at several contact angles is performed to understand the complications that this parameter may add to the stability of liquid film in passive cyclonic separators. With the use of the similar separator geometry shown in Figure 4.1, the other parameters of dimensionless backpressure coefficient, κ, aspect ratio, As, and ratio of axially project area to area of injector nozzle, Γ, are kept at 0.043, 2.3, and 82 respectively. Four cases of contact angle of 0^o, 45^o, 90^o, and 135^o are used to carry out the simulation. At each one of these contact angles, a flow of liquid-only injection is used to develop a stable gas core and liquid film configuration. In order to reach unstable conditions, the volume flow rate is decreased with an incremental change rate of 5% until the liquid film collapsing occurs. The critical case is considered as the case that precedes the collapsing one. Figure 5.30 shows contours of stable liquid film results of all contact angle cases. At contact angle less that 90^o, the liquid phase spreads to cover more area on the walls. This is in fact due to the high wettability of such contact angles. Reverse behavior can be seen for contact angles greater than 90^o as the liquid phase characterizes less spreading and creates partial wetting on the walls. Such wetting behavior make it easier for the contact angle of $< 90^o$ to reach unstable liquid film than the contact angle of $> 90^o$ as shown in next results in Figure 5.27.

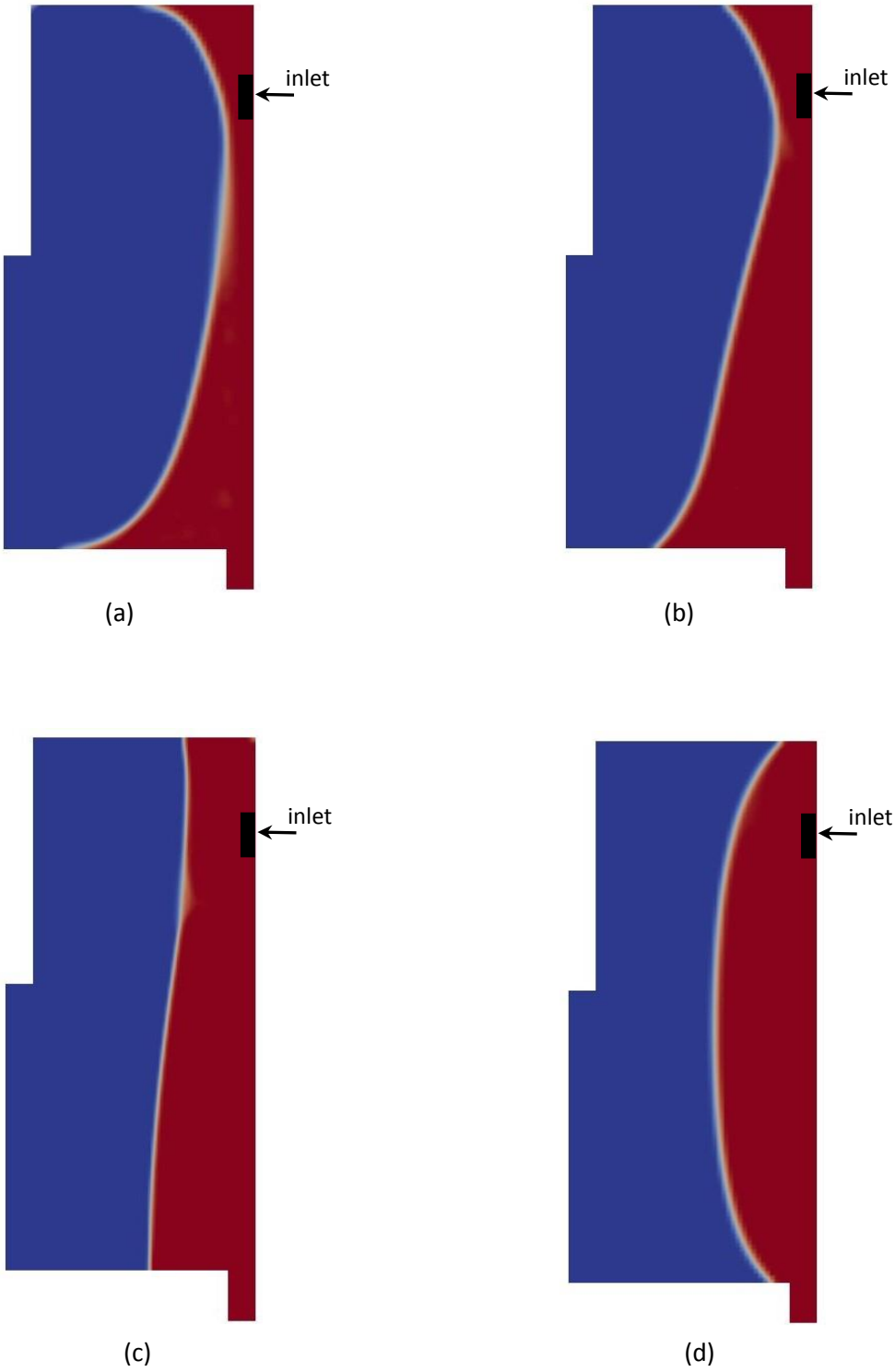

Fig. 5.27 Liquid film contour at contact angles of (a) 0°, (b) 45°, (c) 90°, and (d) 135°

The minimum (critical) injection Weber number is determined and plotted against the contact angle as shown in Figure 5.28.

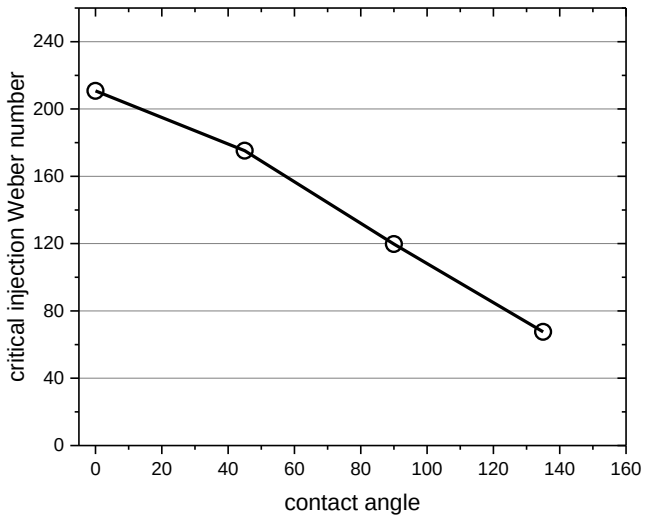

Fig. 5.28 CFD results of critical injection Weber number at several contact angles

It is obvious that by increasing the contact angle the liquid film becomes more stable as the minimum injection Weber number declines.

5.6 Two-Phase Flow Results

All of the previous stability investigations are carried out using liquid-only injection. The scenario is expected to be different if another phase is added to the injected flow. This section investigates this situation using control-volume approximation approach. The investigation is performed using the injection of two-phase flow of air and water at several void fraction values. As the flow tangentially enters the separator housing, the centrifugal force due to angular momentum of the swirl creates buoyancy-like effect and

thus bring the dispersed bubbles toward the gas core where they are collected and subsequently released outside through the gas overflow outlet as shown in Figure 1.1 in Chapter 1. The accumulation of bubbles raises the pressure in the gas core and thus pressure difference is created that pushes the interface as well as the liquid film radially outward. The presence of gas overflow outlet creates backpressure with coefficient of K_g. This coefficient and the backpressure coefficient at the liquid outlet, K_l, play a major rule in in determining the liquid film thickness (Hoyt, Kang, Kharraz, Kadambi, & Kamotani, 2012; Hoyt, Kang, Lee, Kharraz, Kadambi, and Kamotani, 2013). As shown in the pressure balance in Equation 5.16, the pressure due to centrifugal force along with the gas backpressure is balanced by the liquid backpressure and the capillary force caused by surface tension at the interface. Also the conservation of angular momentum at steady state will lead to Equation 5.15.

$$\frac{1}{1-\alpha} = u + \Gamma A_s C_f u^2 \qquad \text{(EQU 5.15)}$$

$$u^2(1-r_i^2) = \frac{2}{We_o r_i} + \kappa_l - \kappa_g \left(\frac{\beta}{1-\beta}\right)^2 \qquad \text{(EQU 5.16)}$$

Parameters of Γ, As and r_i have similar expressions as in single phase injection. While other parameters are identified as $u = \frac{U_\theta}{j_{l,in}}$, $\kappa_l = 2K_l A_{inj}^2$, $\kappa_g = 2\frac{\rho_g}{\rho_l} K_g A_{inj}^2$ and $We_o = \frac{\rho R_o j_{l,in}^2}{\sigma}$.

As the flow rate goes to lower values which leads to liquid film thickening (decrease in gas core) , the capillary force becomes significantly affecting the interface and at certain level

the flow reaches a critical situation where beyond that the liquid film collapses. At the critical situation, the interfacial Weber number is minimum. This situation is achieved analytically as Equations 5.15 and 5.16 are solved simultaneously to obtain r_i, u and We_o in order to calculate We_i afterward. Solving these equation is repeated along with lowering We_o until achieving minimum interfacial Weber number, $We_{i,min}$ where below this value the solution gives negative gas core radius, r_i, value. The skin friction, C_f, is estimated using Equation 5.8 which is the same equation used for single phase. Since Equations 5.15 and 5.16 are in dimensionless form, performing the solution with varying only We_o ensures keeping the other parameters unchanged and thus the effect of any parameters can be studied individually. This solution method in fact is just similar to the one used in liquid-only case. In addition to the parameters introduced in liquid-only injection, two-phase flow has extra two parameters namely void fraction, α, and volumetric quality, β. The results that are introduced in this study is based on the assumption of injecting two-phase flow with no relative velocity between the phases which means $\alpha = \beta$. This assumption can be realistically achieved using homogeneous nozzle which is long enough to allow the two phases to gain similar velocity (Hoyt, 2013). Figure 5.29 shows results obtained using the procedure mentioned above. The change of $We_{o,min}$ is plotted against $Re_o/As^{2.0}$ at several values of void fraction and a specific range of As and k_l . Similar to the case of single phase flow k_l has insignificant effect on the stability of liquid film. Also, the liquid film gains more stability as the injected Reynolds number goes to higher values. Increasing the void fraction makes the flow more susceptible to collapsing.

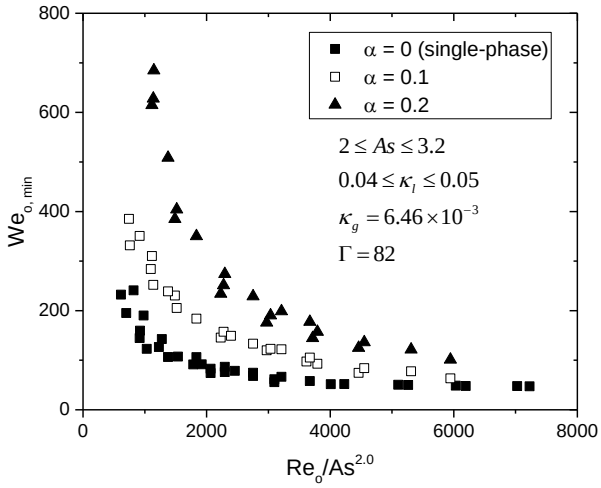

Fig. 5.29 Minimum (critical) injection Weber number using control-volume approximation at several void fraction conditions

Chapter 6 Conclusion and Recommendations

6.1 Conclusion

This work investigates the stability of liquid film in a microgravity environment inside a passive cyclonic separator at a relatively low volume flow rate of liquid-only injection. The effects of surface tension become significant in this situation. Analytical and computational approaches are used to achieve this task. The analytical approach considers only the section above the baffle plate in the separator to carry out a control-volume analysis, and to develop equations that govern the separator hydrodynamics using the conservations of mass and angular momentum as well as a pressure balance equation. This approach is an extension to the Hoyt, et al. (2012) and Hoyt, et al. (2013) works, but in this study the surface tension effect is considered. The CFD approach utilizes the same computational domain that is used in the control-volume analysis. Axisymmetric 2-D meshing is used to perform the CFD simulation.

Since the problem in this study involves a moving free surface (interface), the liquid film thickness is critical in studying the interface stability where for instance, the increase in liquid film thickness causes an increase in the capillary force at the interface which brings the flow closer to encountering instability. Therefore an investigation is performed by conducting a parametric study on the dimensionless parameters that represent the separator geometry and the swirling flow hydrodynamics to determine the effects of all these parameters on the liquid film thickness. Since the liquid film thickness depends mainly on the skin friction coefficient, the current work formulates an expression for this

coefficient at a low volume flow rate injection (low injection Reynolds number) using the CFD simulation data. The developed expression depicts the skin friction coefficient as a function of the liquid film Reynolds number, Re_f.

The developed skin friction coefficient expression is used in the control-volume approximation to carry out stability analysis where two equations (the angular momentum and the pressure balance) are solved simultaneously to obtain values of the thickness and the azimuthal velocity (the maximum value) of the rotating liquid film as the injection Weber number is decreased until no solution can be attained. The critical (minimum) interfacial Weber number is then obtained. For the CFD approach, the injected Weber number is decreased stepwise through increasing surface tension until encountering collapsing. The Weber number just before the collapsing is considered to be the critical case. The critical interfacial Weber number is taken at 10 % away from the baffle plate. The critical condition is presented in terms of the interfacial Weber number and for practical purposes it is presented also in terms of the injection Weber number.

The control-volume analysis predictions agree reasonably well with the CFD results. In comparison to previous work, the obtained critical interfacial Weber number values are much smaller than Bean, et al. (2002) experimental results. They are very close to Samsonov (1971) prediction for the pure solid-body rotation case without injection. All of the above mentioned results of this study are obtained at a 90^o contact angle. Since in a microgravity environment this angle has a significant effect on flow behavior, a qualitative

investigation is conducted to understand and clarify the significance of this parameter in determining the instability of liquid film inside a passive cyclonic separator. The results reveal an important effect of this angle on the minimum (critical) injection Weber number.

The stability of two-phase flow injection is also investigated in this study. The control-volume approximation is used in the investigation. The results are obtained at several values of void fraction with the assumption that there is no relative velocity between the phases in the injected flow. The results show a significant influence of the void fraction on the stability.

The study shows some limits on some parameter ranges. Due to the assumption of right circular cylinder interface in the control-volume analysis, this requires the aspect ratio to be larger than 2. Also, since low injection flow rate is used which led to having laminar flow inside the separator, the obtained skin friction coefficient correlation is limited to injection Reynolds number up to approximately 5×10^4.

6.2 Recommendations

As the present work investigated uses mainly liquid-only injection, thorough research needs to be conducted on two-phase flow injection in order to obtain a full understanding of the liquid film stability in microgravity. The effect of injected two-phase flow pattern should also be investigated.

In the CFD simulation of this study, a 2-D axisymmetric model is used for simplicity. However, the variation in the azimuthal direction may have a role in the instability. Therefore, a 3-D analysis needs to be performed.

The present CFD investigation on the effect of the contact angle on the instability gives limited results. Therefore, a more comprehensive investigation should be carried out to obtain a better understanding of the complicated contact angle effect in rotating flow.

Reduced gravity experimentation should be conducted to obtain physical observation (data) that can be used to validate the CFD results as well as the analytical predictions. At present, microgravity tests on the International Space Station are planned around 2020.

In reduced gravity experiments, extending the range of operability of the separator to lower injection flow rates without collapsing, can be achieved through increasing the surface roughness of the baffle plate. This will change the contact angle which maintains stable liquid film and hence low injection Weber number can be reached.

References

Ahn, H., Tanaka, K., Tsuge, H., Terasaka, K., & Tsukada, K. (2000). Centrifugal Gas-Liquid Separation under Low Gravity Conditions. Separation and Purification Technology, 19:121-129.

Balasubramaniam, R., Rame, E., Kizito, J., & Kassemi, M. (2006). Two Phase Flow Modeling: Summary of Flow Regimes and Pressure Drop Correlations in Reduced and Partial Gravity. NASA/CR - 2006-214085.

Bandyopadhyay, P., & Gad-el-Hak, M. (1996). Rotating Gas-Liquid Flow in Finite Cylinders: Sensitivity of Standing Vortices to End Effect. Experiments in Fluids, 21:124-138.

Bean, D., Waghela, F., Kurwitz, C., & Best, F. (2002). Vortex Necking Phenomenon under Microgravity. Proceedings of the Thermal Fluids Analysis Workshop, NASA Johnson Space Center.

Best, F. (2000). Texas A&M vortex type phase separator. Space Technology and Applications International Forum.

Best, F., & Ellis, M. (1999). Experimental and Analytical results of Liquid-Gas Separator in Microgravity. AIP Conference Proceedings.

Best, F., & Finodeyev, F. (2005). Development of a Passive Flow Coalescence Device for Two-Phase Separation under Microgravity. Proceedings of the Conference of Applications of Thermophysics in Microgravity and Breakthrough Propulsion Physics.

Bhunia, A., & Kamotani, Y. (2001). Flow around a Bubble on a Heated Wall in a Cross-flowing Liquid under Microgravity Condition. *International Journal of Heat and Mass Transfer*, 44:3895-3905.

Boris, J., & Book, L. (1973). Flux-Corrected Transport I: SHASTA, a Fluid-Transport Algorithm That Works. Journal of Computational Physics, Vol. 11, 38-69.

Boudourides, M., & Davis, S. (1986). Stability Criteria for Swirl Flows with Free Surfaces. Journal of Applied Mathematics and Physics, Vol. 37, 597-607.

Brackbill, J., Kothe, D., & Zemach, C. (1992). A continuum method for modeling surface tension. Journal of Computaional Physics, 100:335-354.

Celik, I., Ghia, U., Roache, P., Freitas, C., Coleman, H., and Raad, P. (2008). Procedure for Estimation and Reporting of Uncertainty Due to Discretization in CFD Applications. Journal of Fluids Engineering, Vol. 130, 078001, 1-4.

Chu, K., Wang, B., Xu, D., Chen, Y., & Yu, A. (2011). CFD-DEM Simulation of the Gas-Solid Flow in a Cyclone Separator. Chemical Engineering Science, 66:834-847

Corte, C., & Gil, A. (2007). Modeling the Gas and Particle Flow Inside Cyclone Separators, Progress in Energy and Combustion Science, 33:409-452.

Ellis, M. (2006). The Tangential Velocity Profile and Momentum Transfer within a Microgravity Vortex. MS Thesis, Department of Nuclear Engineering. Texas A&M University, College Station, TX.

Ellis, M., Kurwitz, C., & Best, F. (2005). Development of a Unique Passive Microgravity Vortex Separator. Proceedings of ASME IMECE2005, Orlando, FL.

Escudier, M. (1988). Vortex Breakdown: Observations and Explanation. Progress in Aerospace Sciences, Vol. 25, 189-229.

Gopala, V., & van Wachem, B. (2008). Volume of Fluid Method for Immiscible-Fluid and Free-Surface Flows. Chemical Engineering Journal, Vol. 141, 204-221.

Grigoriev, Y., Grogorov, E., Cykhotsky, V., Prokhorov, Y., Gorbenco, G., Blinkov, V., Teniakov, I., & Malukihin, C. (1996). Two-phase Heat Transport Loop of Central Thermal Control System for the International Space Station ‘‘Alpha’’ Russian Segment. AIChE Symposium Series Heat Transfer, Vol. 310, 9-17.

Hammitt, G., Krzeczkowski, S., & Krzyzanowski, J. (1981). Liquid Film and Droplet Stability Consideration as Applied to Wet Steam Flow, Forschung im Ingenieurwesen, 1:1-14.

Harlow, F., & Welch, J. (1965). Numerical Calculation of Time-Dependent Viscous Incompressible Flow of Fluid with Free Surface, Physics of Fluids, Vol. 8, 2182–2189.

Hirt, C & Nichols, B. (1981). Volume of Fluid (VOF) Method for the Dynamics of Free Boundaries. Journal of Computational Physics, Vol. 39, 201–225.

Hocking, L., & Michael, D. (1959). The Stability of a Column of Rotating Liquid, Mathematika 6:25-32.

Hoffmann, A., & Stein, L. (2008). Gas Cyclones and Swirl Tubes. Springer.

Hoyt, N. (2007). Computational Investigation of the NASA Cascade Cyclonic Separation Device. M.S. Thesis.

Hoyt, N. (2013). The Performance of Passive Cyclonic Separator in Microgravity. PhD Thesis, Department of Mechanical and Aerospace Engineering, Case Western Reserve University. Cleveland, OH.

Hoyt, N., Kamotani, Y., Kadambi, J., McQuillen, J., & Sankovic, J. (2008). Computational Investigation of the NASA Cascade Cyclonic Separation Device. Proceedings of the AIAA 41st Aerospace Sciences Meeting and Exhibition, (pp. AIAA-2008-0809). Reno, NV.

Hoyt, N., Kang, M., Kharraz, A., Kadambi, J., & Kamotani, Y. (2011). Cyclonic Two-Phase Flow Separator Experimentation and Simulation for Use in a Microgravity Environment. Journal of Physics: Conference Series, 327 012056.

Hoyt, N., Kang, M., Kharraz, A., Kadambi, J., & Kamotani, Y. (2012). Dynamic Response of Passive Cyclonic Separator in Microgravity. Proceedings of the 50th AIAA Aerospace Sciences Meeting.

Hoyt, N., Kang, M., Lee, K., Kharraz, A., Kadambi, J., and Kamotani, Y. (2013). Study of Steady and Dynamic Behavior of Gas Core of Passive Cyclonic Separator for Space Applications. Microgravity Science and Technology, 25:187-200.

Huang, Y., & Yang, V. (2005). Effect of Swirl on Combustion Dynamics in a Lean-Premixed Swirl-Stabilized Combustor. Proceedings of the Combustion Institute, 30:1775–1782.

Jasak, H., & Weller, H. (1995). Interface-tracking capabilities of the Inter-Gamma Differencing Scheme. Technical Report, Imperial College, University of London

Kang, M. F., Hoyt, N., Kadambi, J., and Kamotani, Y. (2014). Study of Gas Core Behavior of Passive Cyclonic Two-Phase Separator for Microgravity Applications. Microgravity Science and Technology, 26:147-157.

Kharraz, A., Kang, M. F., and Kamotani, Y. (2016). Stability of the Gas Core of A Cyclonic Two-Phase Separator in Microgravity. Interfacial Phenomena and Heat Transfer, 4(1):71-80.

Kawanami, O., Imai, R., Azuma, H., & Ohta, H. (2004). On-Orbit Cryogenic Fluid Transfer Technique Using Swirl Flow Combined with Condensation by Spray Cooling: Preliminary Study of Microgravity Experiment and Thermal Analysis in Refilling Process, J. Jpn. Soc. Microgravity Appl., Vol. 21, 174-186.

Kawanami, O., Imai, R., Azuma, H., Ohta, H., Honda, I., & Kawashima, Y. (2006). Microgravity Experiment of On-orbit Fluid Transfer Technique using Swirl Flow. Ann. N.Y. Acad. Sci. Vol. 1077, 288–303.

Klein, C. (2009). A Characterization of a Dual Chambered, Two-Phase Separator. MS Thesis, Department of Nuclear Engineering. Texas A&M University, College Station, TX.

Kouba, G., & Shoham, O. (1996). A Review of Gas-Liquid Cylindrical Cyclone (GLCC), International Conference, Aberdeen, UK.

Kubitschek, J., & Weidman, P. (2007). The Effect of Viscosity on the Stability of a Uniformly Rotating Liquid Column in Zero Gravity. Journal of Fluid Mechanics, Vol. 572, 261-286.

McQuillen, J. (2004). Gas Liquid Flows and Phase Separation, Presentation from Strategic Research to Enable NASA's Exploration Missions Conference and Workshop. NASA/CP-2004-213205/Vol.1.

McQuillen, J., & Neumann, E. (1995). Two-Phase Flow Research Using the Learjet Apparatus, NASA Technical Memorandum, NASA, Cleveland, OH, TM 106814, 1-14.

McQuillen, J., Rame, E., Kassemi, M., Singh, B., & Motil, B. (2003). Results of the Workshop on Two-Phase Flow Fluid Stability and Dynamics: Issues in Power, Propulsion, and Advanced Life Support Systems. NASA TM 200-3212598.

McQuillen, J., Sankovic, J., & Hall, N. (2005). Multiphase Flow Separators in Reduced Gravity. Proceedings of IMECE2005, ASME International Mechanical Engineering Congress and Exposition, Orlando, Florida.

Myshkis, A., Babskii, V., Kopachevskii, N., Slobozhanin, L., & Tyuptsov, A. (1987). Low-Gravity Fluid Mechanics, Springer-Verlag Berlin Heidelberg, 120-218, 1987.

Najafi, A., Mousavian, S., & Amini, K. (2011). Numerical Investigations on Swirl Intensity Decay Rate for Turbulent Swirling Flow in a Fixed Pipe. International Journal of Mechanical Science, Vol. 53, 801-811.

Neitzel, G., & Watson, J. (1991). Computational Studies of Vortex Breakdown. Georgia Institute of Technology, AFOSR 91-0047 Final Report.

Nichita, B., Zun, I. & Thomea, J. (2010). A VOF Method Coupled with a Dynamic Contact Angle Model for Simulation of Two-Phase Flows with Partial Wetting. 7th International Conference on Multiphase Flow.

Noh, W., Woodward, P. (1976). Simple Line Interface Calculation. Lecture Notes in Physics, Vol. 59, 330-360.

OpenFOAM. (2013). OpenFOAM User Guide v2.0.1. Retrieved from http://foam.sourceforge.net/docs/Guides-a4/UserGuide.pdf.

Osher, S., & Sethian, J. (1988). Fronts Propagating with Curvature-Dependent Speed: Algorithms Based on Hamilton-Jacobi Formulations. Journal of Computational Physics, Vol. 79, 234–246.

Pedley, T., & Michael, D. (1967). The Stability of Rotating Flows with a Cylindrical Free Surface, Journal of Fluid Mechanics, Vol. 30, 127-147.

Rayleigh, L. (1879). On the Instability of Jets. Proc. London Math. Soc., 10:4-13.

Rayleigh, L. (1892). On the Instability of Cylindrical Fluid Surfaces, Phil. Mag., 34:177-180.

Rezkallah, K. (1995). Recent Progress in the Studies of Two-Phase Flow at Microgravity. *Advances in Space Research*, Vol. 16, No. 7, 123-132.

Rusche, H. (2002). Computational Fluid Dynamics of Dispersed Two-Phase Flow at High Volume Fractions. PhD Thesis, Imperial College of Science. Technology and Medicine, London.

Samsonov, V. (1971). Stability and Bifurcation of the Equilibrium of a Liquid Filled Solid. Nauch. Tr. Inst. Mekh.

Schlichting, H. (1979). Boundary-Layer Theory. McGraw Hill. New York.

Sharp, L., Dietrich, D., & Motil, B. (2013). Microgravity Fluids and Combustion Research at NASA Glenn Research Center. *Journal of Aerospace Engineering*, 26:439-450.

So, K., Hu, X., & Adams, N. (2009). Anti-Diffusion Method for Interface Steepening in Two-Phase Incompressible Flow. Journal of Computational Physics, Vol. 230, 5155-5177.

Supak, K. (2007). Reduced Gravity Rankine Cycle Design and Optimization Study with Passive Vortex. MS Thesis, Department of Nuclear Engineering. Texas A&M University, College Station, TX.

Synge, J. (1938). On the Stability of a Viscous Liquid between Two Rotating Coaxial Cylinders. Proc. Roy. Soc. A 167, 250 256.

Takamasa, T., Iguchi, T., Hazuku, T., Hibiki, T., & Ishii, M. (2003). Interfacial Area Transport of Bubbly Flow under Microgravity Environment. *International Journal of Multiphase Flow,* 29:291-304.

Taylor, G. I. (1923) Stability of a viscous liquid contained between two rotating cylinders, Phil. Trans. Roy. Soc. London A 223, 289-343.

Thomas, E., Graf, J., Sweterlitsch, J., & Weislogel, M. (2008). Development of the Static Phase Separator. SAE Technical Paper 2008-01-2041.

Ubbink, O. (1997). Numerical Prediction of Two Fluid Systems with Sharp Interfaces. PhD Thesis, Imperial College of Science, Technology and Medicine, London.

Unverdi, S. & Tryggvason, G. (1992) A Front-Tracking Method for Viscous, Incompressible Multi-Fluid Flows. Journal of Computational Physics, Vol. 100, 25–37.

van Wachem, B.G.M., Schouten, J. (2002). Experimental Validation of 3-d Lagrangian VOF Model: Bubble Shape and Rise Velocity. AIChE, Vol. 48, 2744-2753.

Wang, S., Gomez, L., Mohan, R., Shoham, O., & Kouba, G. (2003). Gas-Liquid Cylindrical Cyclone (GLCC) Compact Separators for Wet Gas Applications, Journal of Energy Resources Technology, Vol. 125, 43-50.

Weidman, P. (1994). Stability criteria for two immiscible fluids rigidly rotating in zero gravity. Revue Roumaine des Sciences Techniques, Serie de M´ecanique Appliqu´ee, 39:81-496.

Weidman, P., Goto, M., & Fridberg, A. (1997). On the instability of inviscid, rigidly rotating immiscible fluids in zero gravity. Mathematik und Physik ZAMP, 48:921-950.

Weislogel, M., Thomas, E., & Graf, J. (2008). A Novel Device Addressing Design Challenges for Passive Fluid Phase Separations Aboard Spacecraft. Microgravity Science and Technology, 21:257–268

Wu, X., & Chahine, G. (2012). Development of DynaSwirl Phase Separator for Space Applications. Proceedings of the AIAA 50th Aerospace Sciences Meeting.

Yongdong, C. (1997). Studies of Vortex Breakdown and its Stability in a Confined Cylindrical Container. PhD Thesis, Department of Mechanical Engineering, National University of Singapore, Singapore.